Applied Materials Today 34 (2023) 101914

Contents lists available at ScienceDirect

Applied Materials Today

journal homepage: www.elsevier.com/locate/apmt

Review and proposition for model-based multivariable-multiobjective optimisation of extrusion-based bioprinting

Samuel Emebu [a,c], Raphael Olabanji Ogunleye [b], Eva Achbergerová [a], Lenka Vítková [b], Petr Ponížil [b], Clara Mendoza Martinez [d,*]

[a] Department of Automatic Control and Informatics, Faculty of Applied Informatics, Tomas Bata University in Zlín, Nad Stráněmi 4511, Zlín 76005, Czech Republic
[b] Department of Production Engineering, Faculty of Technology, Tomas Bata University in Zlin, Vavrečkova 275, Zlin 76001, Czech Republic
[c] Department of Chemical Engineering, Faculty of Engineering, University of Benin, PO Box 1154, Benin City, Nigeria
[d] Department of Energy, Lappeenranta-Lahti University of Technology LUT, Yliopistonkatu 34, Lappeenranta FI-53850, Finland

ARTICLE INFO

Keywords:
Extrusion-based bioprinting (EBB)
Shearing characteristic
Print resolution (PR)
Cell viability (CV)
Multivariable-multiobjective optimisation

ABSTRACT

Consequent to the development of bioprinting technologies for biomedical applications, especially in tissue engineering, a comprehensive review of extrusion-based bioprinting (EBB) has been written. The review was executed in a manner that laid a foundation for effective optimisation strategies to improve the print resolution or shape fidelity and cell viability of EBB through bioink. However, before achieving this aim the shearing characteristic of the bioink (i.e., shear-thinning or thickening) was described by the Ostwald-de Waele and Herschel-Bulkley models, among other reported models. The dependence of bioink shearing characteristics on temperature and time was also discussed. Emphasis on how these dependencies can be influenced by cross-linking of bioink molecules was further highlighted, which can be covalent (chemical-, photo-cross-linking, etc.) or noncovalent (physical cross-linking, host-guest inclusion, ionic interaction, etc.). Models from literature that can physically describe print resolution and cell viability in EBB were discussed and compared. Therefore, multivariable-multiobjective optimisation strategies were proposed with these models.

1. Introduction

1.1. Precedence of bioprinting

The continual need to improve the potential of regenerative medicine has resulted in the development of bioprinting technologies. Bioprinting is an emerging procedure in tissue engineering proposed for the restoration of living tissues and organs, as well as providing insights into their architectural design and functionality. This advancement in technology has implications for drug development, biocosmetic restoration, revitalisation, etc. [1,2]. In 1988, Klebe first introduced bioprinting as cytoscribing technology, which involved micro-positioning cells and constructing two-dimensional (2D) synthetic tissues [3,4]. Today, bioprinting has evolved to enable the creation of three-dimensional (3D) cell-laden constructs. The traditional approach involves depositing bioink in predefined layered patterns, using a bottom-up assembly method [5,6]. It is based on the principles of stereolithography and additive manufacturing [7]. Some key advantages of bioprinting include the ability to coculture multiple cell types, facilitate controlled delivery of growth factors, and integrate vascularisation within tissues [8–10].

A 3D construct of tissue or organ can follow one of two pathways: either it is incubated in a bioreactor in a controlled environment to mature before being implanted through surgery (*in vitro*), or it is printed directly, utilising the human body as a natural bioreactor (*in vivo*) [16]. To fabricate tissues or organs, the geometry of the constructs can be acquired through an imaging technique such as X-ray, computed tomography (CT), magnetic resonance image (MRI) and ultrasound imaging, Table (1). The gathered image, representing the desired 3D structure, is then fed into computer-aided design (CAD), image-based systems, and implicit surfaces software used to design the internal architecture of the constructs. This software employs sophisticated algorithms and tools to accurately generate structure path plans using a specific algorithm that determines the optimal trajectory and deposition strategy for printing the constructs. Finally, the processed image is converted into specific file formats, such as STL (Standard Tessellation Language) or g-code, Fig. (1a). These files serve as instructions that can be comprehended and executed by bioprinters during the printing process [17].

* Corresponding author.
E-mail address: clara.mendoza.martinez@lut.fi (C.M. Martinez).

https://doi.org/10.1016/j.apmt.2023.101914
Received 24 June 2023; Received in revised form 13 August 2023; Accepted 30 August 2023
Available online 9 September 2023

Table 1
3D imaging techniques with their advantages and limitations.

Imaging Modalities	Types of tissue	Advantages	Disadvantages	Scan time
X-ray imaging [11]	Hard tissue	(a) Less expensive (b)Fast image acquisition (c) Widely available	(a) Limited soft tissue visualisation (b) Ionising radiation (c) Lack of real-time imaging	Seconds
Computed Tomography (CT) [12]	Hard tissue	(a) High-resolution imaging (b) Fast image construction (c) Multiplanar imaging with comprehensive visualisation (d) Versatile applications	(a) Expensive (b) Ionising radiation (c) Limited soft tissue contrast	Minutes
Magnetic Resonance Imaging (MRI) [13]	Hard and soft tissue	(a) Excellent soft tissue contrast (b) Non-ionising radiation (c) Multiplanar imaging capability (d) High spatial resolution	(a) Longer scan time (b)Limited availability, and expensive (c)Less effective for bone imaging	Minutes to hour
Ultrasound [14]	Hard and soft tissue	(a) Non-ionising radiation (b) Cost-effective (c) Dynamic tissue assessment	(a) Challenging in capturing images complex organ (b) Limited penetration and resolution	Minutes
Optical Coherence Tomography (OCT) [15]	Hard and soft tissue	(a) High-resolution imaging (b) Non-invasive and non-ionising	(a) Limited imaging depth compared to CT and MRI (b) Limited field of view	Minutes

1.2. Bioprintable materials

In cartilage tissue engineering, such as cartilage and bone bioprinting, the bioprinted constructs must possess adequate mechanical stability, including strength, stiffness, and wear resistance, as well as favourable biological characteristics [18]. The materials used for this type of bioprinting may require higher processing temperatures and pressures in the presence of organic solvents [19]. These materials, which do not accommodate living cells, are appropriately referred to as biomaterial inks [5]. While both bioink and biomaterial ink can be considered bioprintable materials, this review focuses on bioink as the primary bioprintable material of interest. The distinction between these two types of bioprintable materials lies in their ability to encapsulate living cells [5,7,18–21].

Bioinks are bioprintable materials that encapsulate living cells within printable hydrogels. These hydrogels are cross-linked polymeric matrices prepared from natural or synthetic materials, with a preference for biopolymers due to their good biocompatibility, biodegradability, and ability to mimic the extracellular matrix. Examples of biopolymers used in hydrogel bioinks include hyaluronic acid (HA) [22], alginate, fibrin, gelatin, collagen, and gelatin methacryloyl (GelMA) [22–24]. On the other hand, biomaterial inks are aqueous formulations of polymers or hydrogel precursors that may contain biological factors but do not include living cells [5,7,19,20]. They are primarily used for creating mechanically stable scaffolds and implants, to which cells are subsequently introduced [7]. Typical examples of biomaterial inks include thermoplastic polymers like polycaprolactone (biodegradable), polypropylene (non-degradable), polyoxazolines (thermoresponsive non-degradable), and biopolymers such as gelatin and fibronectin [20,21].

Hydrogels are commonly employed in the formulation of both bioinks and biomaterial inks due to their remarkable ability to absorb and retain significant amounts of water without dissolving [25]. The hydrophilic functional groups in hydrogels contribute to their water-absorbing capabilities, while the crosslinking of polymer chains ensures their resistance to dissolution. Hydrogels exhibit biocompatibility, biodegradability, and a close resemblance to natural tissue structures. Table (2) provides a list of typical natural and synthetic biomaterial hydrogels used as bioinks in tissue engineering applications. Natural biomaterial-derived hydrogels offer notable advantages, such as excellent biocompatibility, biodegradability, and biochemical components that promote cell adhesion [26,27]. However, they may have limitations in terms of mechanical properties and batch-to-batch variability, which can reduce experimental reproducibility [28]. Synthetic polymers, on the other hand, offer tuneable and highly reproducible mechanical properties but often lack the intrinsic biological motifs required for cell adhesion. They may also pose challenges for enzymatic modification and remodelling [29]. Nevertheless, researchers have addressed these limitations by exploring chemical modification or incorporating biomolecules into synthetic polymers to enhance their bioactivity [30].

1.3. The characteristic expectation of bioprintable materials

In summary, bioprintable materials, whether with or without cells, can be enhanced by incorporating biologically active components to improve the biochemical, rheological, and mechanical properties of the printed constructs. An ideal bioprintable material should possess

Table 2
Some common bioinks used in tissue engineering.

Bioink	Cell types	Applications
Natural biomaterial based		
Alginate [31]	Chondrocytes	Cartilage
Gelatine [32]	Fibroblasts	Skin
Collagen [33]	Fibroblasts	Skin
Fibrin [34]	Platelets	Wound healing
Hyaluronic Acid [35]	Mesenchymal stem cells	Cartilage, Nerves
Matrigel [36]	Cancer cells	Cancer research
Chitosan [37]	N/A	Bone, cartilage
Synthetic biomaterial based		
Polyethylene Glycol (PEG) [38]	N/A	Bone, nerves
Polycaprolactone (PCL) [39]	Osteochondral	Cartilage
Poly (lactic acid) (PLA) [40]	Mesenchymal stem cell	Scaffolds
Poly (lactic-co-glycolic acid) (PLGA) [41]	Mesenchymal stem cell	Bone
Polyvinyl alcohol (PVA) [42]	N/A	Scaffolds

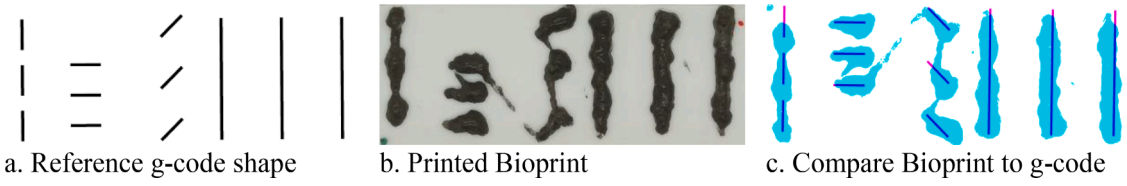

Fig. 1. Typical illustrations of g-code shape, Bioprint and their comparison.

properties that facilitate its processability in achieving bioprinting objectives: (a) Generation of tissue constructs with adequate mechanical strength and robustness while maintaining compatibility with the mechanics of the target tissue; (b) Ability to undergo adjustable gelation and stabilisation processes, enabling high precision and shape fidelity; (c) Biocompatibility and biodegradability that closely mimic the natural microenvironment of the tissues; (d) Suitability for chemical modifications to address the specific requirements of different tissue types; (e) Potential for large-scale production, minimising batch-to-batch variations; (f) Shear-thinning behaviour to protect cells from high shear stress during printing [22,43,44]. Therefore, the key to successful bioprinting lies in determining the optimal formulation of bioprintable materials. Especially for cell-laden bioink, where biological characteristics such as cytocompatibility, cell proliferation, and cell adhesion are critical [22]. Since adequate cell viability in the bioprint must be achieved, attaining these highlighted objectives is more difficult for cases of 3D bioprinting with bioink, compared to traditional 3D printing without bioink [22,43,45–47].

Two critical factors that need to be monitored and controlled for bioink during bioprinting are shape fidelity (an evaluation of the structural differences between the design and actual bioprint [43], Fig. (1c)) and cell viability (a measure of the proportion of living cells in the bioprint [48]) [49]. It is important to note that shape fidelity depends on print resolution, which measures the uniformity of bioink thickness over the smallest unit, such as a line or arc, in the bioprint filament. Print resolution significantly contributes to overall shape fidelity [50]. Various factors and decisions before (e.g., composition of bioinks including materials, types of living cells, and additives), during (specific bioprinting methods and parameters, *in situ* cross-linking, etc.), and after (specific type and degree of cross-linking) the bioprinting process can affect these responses [51].

1.4. Methods of bioprinting, extrusion-based bioprinting (EBB), a clear-cut method

The method of bioprinting plays a crucial role in determining how shape fidelity and cell viability can be evaluated. This is because the bioprinting process is typically constrained by the available equipment, tools, and allowable range of operational parameters. The following are established bioprinting methods: Droplet-based bioprinting (DBB), which encompasses inkjet-based bioprinting, acoustic droplet ejection, and microvalve-assisted bioprinting principles [52]; Extrusion-based bioprinting (EBB), which can be further categorised into mechanical microextrusion, pneumatic microextrusion, and solenoid microextrusion [53]; Light-based bioprinting (LBB), which is based on either laser or digital light processing principles [54]; Magnetic bioprinting [55]; and Stereolithography (SLA) Bioprinting [56]. Comprehensive details on the working principles of these highlighted methods were reviewed by Adhikari et al. [7]. The capabilities, advantages and disadvantages of some of these methods are summarised in Table (3).

In Inkjet-based Bioprinting, bioinks are loaded into inkjet cartridges, and droplets are accurately deposited onto a substrate or scaffold using thermal or piezoelectric drop-on-demand delivery methods [57]. This innovative approach enables the printing of bioinks without requiring direct contact between the delivery nozzle and the receiving surface, minimising the risk of contamination. The non-contact printing method offers several advantages, particularly in terms of precision and versatility. By incorporating multiple print heads, each containing a specific bioink or cell suspension, it becomes possible to create complex structures with spatially controlled distribution of different biomaterials or cell populations [58,59]. This capability opens exciting possibilities for fabricating intricate tissues or organ-like constructs that closely mimic the complexity and diversity found in natural biological systems.

Laser-assisted bioprinting is an advanced technique that utilises laser energy to deposit bioinks with exceptional precision and control, offering unique advantages for printing delicate structures while maintaining cell viability. In this method, a pulsed laser is focused onto a material called a “donor layer” which contains the bioink [60]. The laser energy rapidly increases pressure, creating tiny droplets or bioink jets propelled towards a receiving substrate, often called the “collector plate”. This process is known as “laser-induced forward transfer”. One of the main advantages of laser-assisted bioprinting is its ability to deposit bioinks without direct contact, minimising the risk of damage or contamination. The precise control over laser parameters, such as pulse energy, duration, and focal point, allows for accurately placing bioink droplets or jets onto the collector plate. This level of control enables the creation of intricate and complex structures with high resolution [60,61].

Stereolithography (SLA) Bioprinting is an advanced bioprinting

Table 3
Bioprinting techniques with their advantages and limitations.

Bioprinting Techniques	Advantages	Disadvantages	Resolution, μm	Speed
Inkjet-based Bioprinting [72]	(a) High resolution (precise deposition of tiny droplets of bioink) (b) Versatility in cell types and Bioinks (c) Non-contact printing (reduced tendency of delicate cells or structures damage) (d) Suitability for high-throughput applications (e) Control over cell density and patterning (f) low cost	(a) Limited to low viscosity bioinks due to small nozzle size (b) Cell viability challenges due to mechanical stresses, shear forces, and changes in temperature (c) Low and limited cell density (d) Difficulty in printing complex structures (e) Limited structural integrity	$<$ 5 to 500	1-10,000 droplet.s^{-1}
Extrusion-based Bioprinting [63]	(a) Compatible with wide ranges of bioinks (b) Control over cell density (c) Ability to print high viscosity bioinks	(a) Low cell viability (b) Limited biomaterial due to shear thinning requirement (c) A long production time	100-500	10-50 μm. s^{-1}
Laser-assisted Bioprinting [60]	(a) High precision (up to nanoscale) and resolution (b) Non-contact printing (less risk of contamination and damage to printed structure) (c) Minimal shear stress on cells (d) Compatibility with a wide range of bioinks	(a) Low printing speed (b) Low printing depth (c) Expensive (d) Possible cell and tissue damage due to UV light	20 - 100	$\cong$10,000 droplet.s^{-1}
Microvalve-based Bioprinting [73]	(a) High precision and resolution (b) Versatile bioink compatibility (c) Printing of complex and detailed structures	(a) Limited viscosity range of bioinks (moderate to high viscosities) (b) Risk of clogging (c) Potential for cross-contamination	50 - 500	0.5-50 mm. s^{-1}
Magnetic Bioprinting [55]	(a) Minimum risk of damage or contamination due to the non-contact printing method (b) Versatile bioink compatibility (c) High cell viability (d) Excellent precision and resolution	(a) Limited printing depth (b) Reliance on magnetic properties	2 - 100	5-50 mm. s^{-1}
Stereolithography (SLA) [56]	(a) High precision (b) Relatively fast production (c) Good cell viability due to the short exposure to UV or laser light	(a) Requires support structures to prevent deformation (b) High maintenance cost of the components (c) Material limitations (primarily suitable for the photosensitive resin)	10 - 100	$\geq$ 700 mm. hr^{-1}

technique that provides unique capabilities for fabricating complex biological structures. It operates based on the principle of photopolymerisation. A liquid bioink containing photopolymerisable components, such as hydrogels or resins, is exposed to a specific pattern of light, typically ultraviolet (UV) light. This light initiates a polymerisation reaction, causing the liquid bioink to solidify and form a layer. The process is repeated layer by layer, with each subsequent layer being cured and bonded to the previous layer. This layer-by-layer approach allows for the creation of intricate and precise three-dimensional structures with high resolution [56]. SLA bioprinting excels in achieving excellent details and high resolution, making it suitable for printing complex structures at the cellular and subcellular scale. It enables the production of intricately structured scaffolds, microfluidic channels, and other features that mimic the complexity of native tissues [62]. SLA bioprinting continues to advance and holds great promise for tissue engineering, regenerative medicine, and biomedical research.

Extrusion-based bioprinting is another widely employed technique in bioprinting. This approach involves extruding bioink through a nozzle or printing head using controlled pressure or mechanical forces, as shown in Fig. (2a), (2b). Extrusion-based bioprinting offers several advantages, including versatility in bioink selection and the ability to incorporate various biomaterials and cells. By carefully controlling the extrusion process, it is possible to deposit the bioink layer by layer, ultimately building a three-dimensional structure with precise control over its internal architecture [63].

Having highlighted and discusses the various bioprinting techniques, this work will focus specifically on Extrusion-based bioprinting (EBB) and explore strategies for its optimisation. The intricacies of EBB, including its key components, working principles, and various parameters that can be fine-tuned for improved cell viability and shape fidelity, will be discussed. Unlike other bioprinting techniques like Droplet-based bioprinting (DBB) and EBB, where the mechanism of bioink delivery is governed by physical contact, EBB presents challenges to cell viability primarily due to factors such as droplet size, impact velocity of the bioink delivery, heat generation, and nozzle clogging [64].

Shear stress is a significant influencing factor in EBB [7]. Operational factors such as nozzle geometry, nozzle diameter, and extrusion pressure or velocity play a crucial role in determining the magnitude of shear stress in EBB. EBB is a popular bioprinting method due to its clear-cut procedure, simplicity, diversity, and predictability [65]. It is capable of printing bioinks of a wide range of viscosities (30 mPa.s to over 6×10^7 mPa.s) and can create large-scale three-dimensional models in centimetre-scale with high cell densities ($>10^8$ cells.mL^{-1}) [46].

The implementation of EBB relies on various operational parameters; (a) Extrusion pressure or velocity; (b) Nozzle geometry (i.e., cylindrical, or conical, convergence angle of conical geometry [66]) and nozzle diameter; (c) Cartridge temperature and platform temperature; (d) Axial velocity of the printhead in the x- and y-direction; pre-flow and post--flow time; (e) Path-height and path-space [47,67–71]. These parameters directly impact bioprint resolution (the precision of the bioink filament) [47], consequently its shape fidelity, as well as cell viability through changes in bioink shear stress. The definitions of these preceding operational parameters are summarised: Nozzle geometry refers to the shape of the printer nozzle (either cylindrical or conical), while nozzle diameter represents the diameter of the nozzle. Axial velocity denotes the velocity of the bioprinter's head, and extrusion velocity is the velocity of the bioinks as they are extruded from the nozzle tip. Pre-flow and post-flow time refer to the duration of bioink extrusion stoppage and continuation at each printing interval. Path-height represents the height between the bioprint filament and the nozzle tip, while path-space refers to the spacing between two adjacent bioprint filaments on the printing platform.

1.5. Research gap, aim and objectives

In Extrusion-based bioprinting (EBB), there is a trade-off between low shear stress, which is necessary for higher cell viability, and high shear stress, which is required for higher print resolution and shape fidelity using the same bioink [47]. This indicates the need to find an optimal shear stress value that can simultaneously maximise bioprint cell viability and print resolution [46]. As two responses need to be optimised by manipulating the operational parameters mentioned earlier, a multivariable-multiobjective optimisation strategy becomes necessary. However, most literature on EBB optimisation focuses on factor-by-factor and single-objective optimisation strategies [47,74–76]. Therefore, given this research gap, this work aims to review models that can predict EBB responses based on its operational parameters. And based on the adequacy of these models, an effective strategy can be proposed for conducting a multivariable-multiobjective optimisation of EBB.

1.6. Applicable models and model adoption

In performing the multivariable-multiobjective optimisation of EBB, the reliability of the deduced optimal condition is significantly dependent on the adequacy of models relating the EBB operating parameters and responses. Therefore appropriate procedures or methodologies must be employed to develop the required EBB models. The EBB models can be developed as mathematical models (i.e., statistical, analytical and trend-based models) as well as machine learning models. Statistical models can be considered as the generic multivariable regression models, developed based on the statistical significance (i.e., a probability value of less than 5%) of operating parameters to a specific response [77] through methods such as the Design of experiments (DOE). Analytical models are models developed based on precise mathematical relations of operating parameters and response, deduced from established physical theories, laws, as well as principles governing the EBB operations [78] (e.g. via material, and energy balances). Trend-based models are models developed with the priority to fit the trend of a data set through curve-fitting software and/or tools. The resulting models are a generic cluster of models encompassing exponential, polynomial, multivariable regression, power law, gaussian etc.

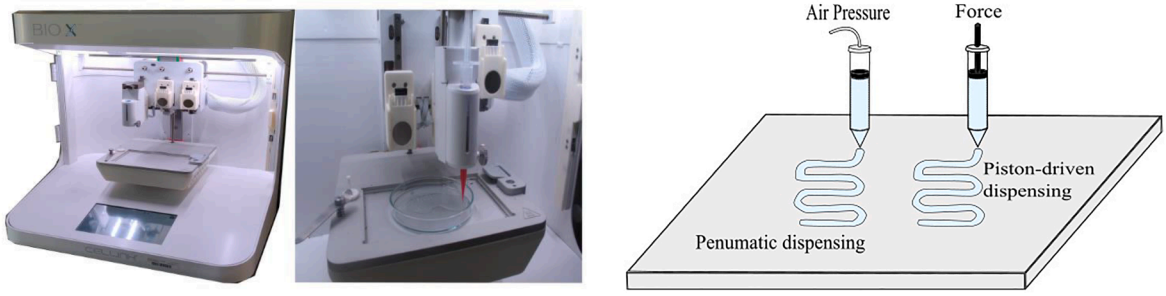

a. Typical EBB bioprinter

b. Typical operational modes of EBB

Fig. 2. Visual illustration of EBB bioprinter and operational modes.

[79], with no precise analytical relationship. While machine learning models are algorithm-based models in which a computing system learns from data and uses algorithms to predict the resulting EBB responses without explicit mathematical relationship [80].

The numbers, and specific operating parameters to be modelled to an EBB response, determine the type of EBB model that can be applied, as well as the complexity of the modelling approach [81]. The mathematical modelling approach [82,83] and machine learning approach are well reported in EBB [84–86]. Table (4) highlights the advantages and as well as limitations of machine learning and mathematical modelling. The mathematical modelling approach will however be applied in modelling the EBB in this work. The reason is predominately based on the highlighted features of mechanistic understanding and interpretation, data requirement, transferability, as well as computational time and resources. Typically, in regards to data requirement, report [87] indicates that machine learning requires a minimum of about 1000 data points [88] for training and testing. Tröndle et al. [89] for example applied 4974 for automated toxicity testing with bioprinted renal spheroids.

2. Characterisation of the rheological property of bioink

When implementing and evaluating bioprinting, it is important to perform a prior investigation of the bioink printability, which can be determined from its shearing characteristics. This investigation enables the development of the bioink within the operational limits of available bioprinters and printing accessories, such as nozzle geometry and diameter [44]. The shearing characteristic of a bioink refers to its flow behaviour under applied pressure. Bioink can exhibit shear-thinning or shear-thickening, where the apparent viscosity decreases or increases, respectively, with an increase in shear rate. This behaviour is typical of non-Newtonian fluids. In EBB applications, shear-thinning behaviour is generally desired as it improves the flow of the bioink, and most bioinks exhibit this property [23,92–94].

Table 4
Comparison of mathematical and machine learning models for bioprinting process [90,88,91].

Features	Machine Learning Model	Mathematical Model
Mechanistic understanding and interpretation	Models are based on statistical patterns and correlations found in the data. While they can be powerful for pattern recognition, their optimisation landscape can be difficult to interpret, making it challenging to understand why specific parameter settings are preferred.	They are based on fundamental laws and principles that can provide more direct insights into how different parameters impact the bioprinting process.
Data requirement	Require a large amount of high-quality training data to perform well. However, the biomedical nature of the bioprinting process makes obtaining large amounts of data challenging.	Require less experimental data for calibration and validation.
Transferability	A model trained on a specific bioprinting system depends primarily on the features of training data. Therefore, it might not function efficiently for a different bioprinter, materials or experimental setup.	If formulated accurately, mathematical models based on physical equations can offer transferable insights and optimisation strategies across various bioprinting platforms.
Computational time and resources	Training complex machine learning models can be computationally expensive and time-consuming, especially for 3D printing applications.	In contrast, optimising explicit physical equations may involve simpler and faster computational methods.
Expert knowledge incorporation	Knowledge and expertise used in developing its models are represented implicitly in the data. They might require additional efforts to describe explicitly for improvement.	Allow researchers to incorporate domain knowledge and expertise directly into model formulations.

The shearing characteristic of a bioink is often mathematically described using the Ostwald-de Waele or Power-law model, Eq. (1) [19], based on experimental data of shear stress, τ, and shear rate, $\dot{\gamma}$. The Herschel-Bulkley model, Eq. (2) [19,95] can also be applied, which in addition accounts for wall slipping through consideration of yield stress, τ_o. The yield stress is the minimum pressure that initiates the flow of bioink [96]. Shear stress is the mechanical force that causes the deformation of bioink's composite structure along the plane parallel to the direction of the stress. While shear rate is the rate at which a progressive shearing deformation is applied. Where k is the flow consistency index, and n is a dimensionless flow behaviour index. The shear stress can also be expressed in terms of the bioink shear rate and apparent viscosity, η, as given by Eq. (3).

$$\tau = k(dv/dr)^n = k\dot{\gamma}^n \quad (1)$$

$$\tau = \tau_o + k(dv/dr)^n = \tau_o + k\dot{\gamma}^n \quad (2)$$

$$\tau = \eta(dv/dr) = \eta\dot{\gamma} \quad (3)$$

The Ostwald-de Waele [47–52] and Herschel-Bulkley model [97–102] are popular simplified models reported in literature to evaluate and validate bioink shearing characteristics. It has been frequently reported that $n < 1$, i.e., a definition of shear-thinning. Note that $n > 1$ signifies shear-thickening, and $n = 1$ implies a Newtonian fluid [19,103], as depicted in Fig. (3). In addition to these two models, there are other models available, such as the Cross, Carreau-Yasuda, and Carreau-Gahleitner models [104–106].

Most of the properties of bioink are temperature-dependent, as such and temperature variations can significantly alter these properties [107]. It is widely reported in literature that bioink viscosity generally decreases with increasing temperature [48,108–113]. Although a reverse scenario to this claim has been reported, where increased temperature enhances physical cross-linking to strengthen the bioinks structure [101,114] while still retaining its shear-thinning characteristic. Given these observations, it is crucial to quantify the rheological changes of bioink with temperature. However, there is limited literature available on the mathematical evaluation of these phenomena, except for the study by Magalhães et al.[71], which considered the Ostwald-de Waele model with an exponential ratio of temperature. Li et al. [112] graphically demonstrated the changes in flow consistency index, k, and flow behaviour index, n, with respect to temperature. A more appropriate approach to account for temperature dependences would be to follow the premise of Gabas et al. [115] report for goat milk, where the parameters (flow consistency index, k, flow behaviour index, n, yield stress, τ_o and apparent viscosity, η) for bioinks can be modelled using the Arrhenius model, Eq. (4). Where A_0, E_a, R and T are pre-exponential factors, activation energy, ideal gas constant and temperature, respectively. In a similar procedure, Abu-Jdayil et al. [116] reported on labneh rheological properties, and modelled its apparent viscosity, η, with Eq. (4), while the flow consistency index, k, and flow behaviour index, n, were modelled with Eqs. (5) and (6) respectively. These approaches could be applied to bioinks. Where a, b, c, α, and ℓ are curved fitted constants dependent on the nature of the specific bioink.

$$k, n, \tau_o, t, \eta = A_0 \exp(E_a / RT) \quad (4)$$

$$\ln k = a + bT + cT^2 \quad (5)$$

$$n = 1 - \alpha/(T + \ell) \quad (6)$$

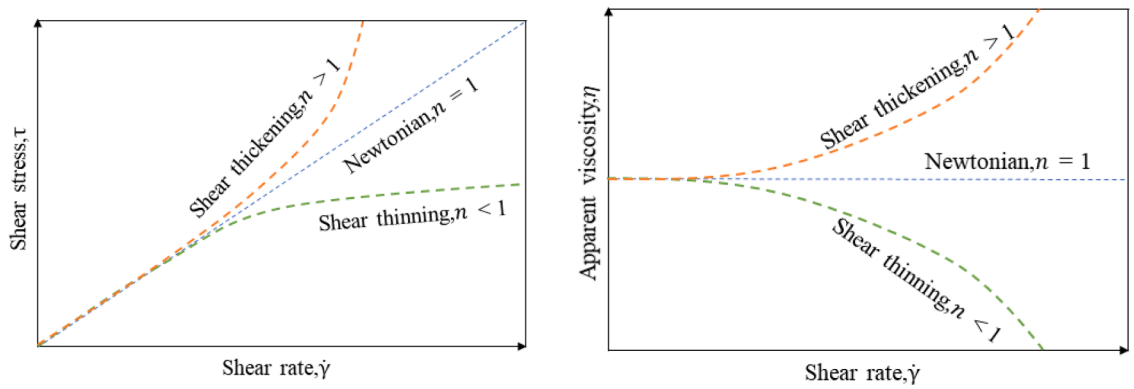

Fig. 3. Graphical illustration of the relationship of shear rate with stress and viscosity.

Eq. (5) models the flow consistency index, k, as an exponent of the quadratic relation of the fluid temperature, like Eq. (4). On the other hand, the flow behaviour index, n, in Eq. (6) is an inversely proportional model that assumes the bioink shearing characteristic would be Newtonian (n = 1) at a specific high-temperature limit, such that the term $\alpha/(T+\alpha)$ would be approximately zero based on the decimal points considered. While Eq. (4) is adequate for modelling all the above-stated rheological parameters from a mathematical standpoint, Eq. (6) may be more suitable for the flow behaviour index, n, from a physical interpretation standpoint. However, the decision on which equation to use for any of these rheological parameters should be based on the model that fits the experimental data best.

Furthermore, in addition to temperature dependence, bioink shearing characteristics can also be time-dependent. Specifically, the apparent viscosity can either decrease with time on shearing (thixotropic) or increase with time (rheopectic) [117]. A thixotropic bioink is usually desirable for EBB if thixotropy occurs within a short time. It is important for bioink viscosity to steadily decrease on the application of shear rate and rapidly recover on termination. This implies that for EBB, extrusion of bioink through a narrow printer nozzle can be achieved without necessarily increasing the shear stress [23,93]. Following the Abu-Jdayil et al. [116] report for labneh, the Waltmann model could also be used to describe thixotropy bioink as given by Eq. (7), which relates how the shear stress, τ changes with time, t. Moreover, it is expected that the timing characteristic of bioink thixotropy will be temperature dependent, which can be modelled by Eq. (4) as described by Ouyang et al. [118] for a so-called gelation time, which declines with the decrease in temperature. It should be noted that models with time, t, Eqs. (4) and (7) describing thixotropy are not expected to affect bioprint quality significantly, but rather, it eases the bioprinting process and enhances the post-printing properties of bioprint. Also, based on its temperature dependence, it is expected to be influenced by platform temperature.

$$\tau = A - B\ln t \tag{7}$$

2.1. Cross-linking of bioink

Having highlighted the temperature dependence and thixotropy of bioink, it should be stated that enhanced molecular interactions inside the bioink could influence the temperature dependence and thixotropy behaviour of bioink [101,114]. Different molecular interactions, resulting in cross-linked matrix (thus the gelation of bioink) are usually necessary for the maintenance of bioprint shape fidelity and cell viability [69,119,120]. This enhanced molecular interaction is termed cross-linking – it is the formation of bonds between polymeric chains in the bioink. Cross-linking can be initiated before or after the bioprinting process (i.e., pre- or post-cross-linking) [119]. Post-cross-linking is favourable for bioinks with high enough viscosity to maintain their shape fidelity after bioprinting [77], while pre-cross-linking is suitable for bioprint, which exhibits instability of shape fidelity (because of low viscosity) after bioprinting [121]. This viscosity yardstick highlighted in these definitions buttresses how bioink cross-linking kinetics could be monitored [122–124].

Typical classification of cross-linking includes physical and chemical cross-linking. In the case of physical cross-linking, it is the result of non-covalent bond formation or weak interactions, which can be: host-guest inclusion (such as the supramolecular host-guest interactions [125]); ionic interaction (often with divalent cation, such as Ca^{2+}, $Mg^{2+}$and Ba^{2+} [126]); hydrophilic and hydrophobic interactions; hydrogen bonds etc. [127–130]. The resulting materials are characterised by poor mechanical stability, and the cross-linking network is reversible [127,128,131]. On the other hand, chemically cross-linked hydrogels are formed by covalent bonds, thus providing irreversible and strong interaction with the polymeric matrix. A covalently cross-linked network can be initiated by: chemical reagents, which may be cytotoxic; enzymatic reactions; ultraviolet photopolymerisation etc. [7,43,69,132]. A comprehensive review of cross-linking has been reported in literature [7,132,133].

3. Relationship among operational parameters and with responses in EBB

Extrusion-based bioprinting (EBB) involves the use of a cartridge or syringe filled with bioink. It relies on applying controlled pressure to the loaded cartridge, which then extrudes the bioink through a nozzle onto the bioprinter platform, as shown in Fig. (5). Based on existing research in literature, it has been observed that the operational parameters (such as extrusion pressure or velocity, nozzle geometry, nozzle diameter, cartridge temperature, platform temperature, axial velocity, pre-flow time, post-flow time, path-height and path-space) exhibit proportional, inverse, joint, and combined relationships with the printer responses (i.e., print resolution and cell viability). exhibit proportional, inverse, joint, and combined relationships with the printer responses [49], as depicted in Fig. (4). Consequently, the precise exposition of these relationships, as reported in the literature will be discussed. The primary influencing factor on both print resolution and cell viability in EBB is

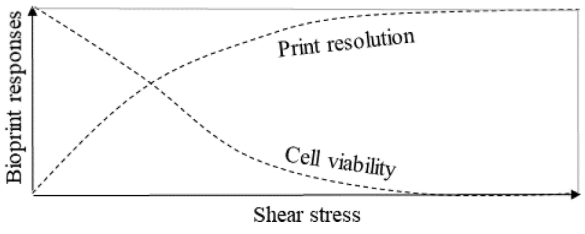

Fig. 4. Illustration of the impact of shear stress on bioprint responses.

shear stress [81,134], which is determined by the fluid mechanics and rheology of the bioink being extruded through the printer nozzle. Therefore, in EBB, the shear stress experienced by a bioink with known rheological properties is influenced by the bioprinter nozzle (i.e., its geometry and diameter), extrusion pressure or velocity, and cartridge temperature [74,110,135].

High shear stress is a significant cause of cell death in EBB [92]. Therefore, achieving low shear stress is crucial for promoting higher cell viability in bioprinting [47], indicating an inverse relationship between shear stress and cell viability. The following approaches can help in reducing shear stress: (a) Application of lower extrusion pressure at a constant temperature, using a specific nozzle geometry and diameter; (b) Use of a larger nozzle diameter for a specific nozzle geometry at a constant temperature and pressure; (c) Application of a higher cartridge temperature (within a safe limit to avoid cell damage) at a constant pressure, using a specific nozzle geometry and diameter; (d) Changes in nozzle geometry for a specific nozzle diameter at a constant temperature and pressure [7,66,110,136]. Regarding nozzle geometry, using a conical nozzle instead of a cylindrical one offers advantages in terms of lower shear stress. In this case, the bioink's shear stress increases towards the outlet region of the conical geometry and is highest at its tip, thus reducing cells' exposure time to high shear stress [7]. The explanations provided above demonstrate that nozzle diameter and temperature generally have an inverse relationship with shear stress, while extrusion pressure has a proportional relationship. It is important to note that the relationship between temperature and shear stress, and consequently cell viability, should be carefully managed. Increasing the cartridge temperature can lower shear stress by reducing the viscosity of the bioink [110]. However, temperature should be controlled within a certain limit to avoid damaging the bioink cells.

Furthermore, in contrast to cell viability, a higher print resolution requires high shear stress, indicating a proportional relationship. As a result, cell viability and print resolution exhibit a competitive relationship with shear stress. In addition to the previously mentioned parameters (extrusion pressure or velocity, nozzle geometry, nozzle diameter, and cartridge temperature), other factors such as axial velocity, pre-flow time, post-flow time, platform temperature, path-height, and path-space can also influence shear stress [67,137,138]. Literature reviews have discussed the impact of these additional parameters on shear stress.

It is generally suggested that axial velocity should be selected interactively with the extrusion pressure or velocity [66]. Lower extrusion pressure requires slower axial velocity, while higher extrusion pressure necessitates faster axial velocity to achieve higher print resolution [23,96,97]. Consequently, it has been recommended to adjust the extrusion velocity to match the axial velocity [139–141]. However, this assertion is debatable as Attalla et al. [139] observed that the relationship between extrusion velocity (or pressure) and axial velocity is often nonlinear due to the non-Newtonian behaviour of bioink. Therefore, while extrusion velocity and axial velocity may be proportional, they are not necessarily equal. Although Heile et al. [142] reported that faster axial velocity and slower extrusion velocity resulted in higher print resolution, further investigation is needed to confirm this relationship. It should be noted that the independent impact of extrusion velocity on bioprinting responses has not been extensively discussed, as it can be inferred from the extrusion pressure at a given nozzle geometry, nozzle diameter [46,142–144], and, to some extent, the cartridge temperature (considering the dependence of bioink shearing characteristics on temperature, as discussed earlier).

The pre-flow and post-flow times are related to the axial velocity and can affect print resolution (or shape fidelity) [145], although the specific relationship has not been reported in literature. Platform temperature is important for post-printing cell viability, as a significant temperature difference between the cartridge and platform can cause thermal shock to cells. It has been reported that printing on a non-heated platform results in lower shape fidelity compared to a heated platform [36].

Regarding path-height and path-space, reports indicate they interact with extrusion pressure and nozzle diameter. Increasing extrusion pressure requires a corresponding increase in path-height and path-space. Path-height and path-space are chosen relative to the nozzle diameter [146]. An excessively high path-height can lead to incomplete or thinner bioprints since the extruded bioink may not make proper contact with the platform. On the other hand, a path-height that is too low can disrupt the bioprinting process as the print nozzles may collide with already layered bioprint patterns, thereby affecting shape fidelity [137].

To summarise the discussion on the operational parameters of EBB regarding shear stress and its relationship with the two highlighted responses, it can be inferred that cell viability and shape fidelity have a significant competitive relationship. Therefore, it is important to find compromise or optimal values for the operating parameters that simultaneously maximise shape fidelity and cell viability or minimise their trade-offs [46].

3.1. Modelling the theoretical prediction of EBB bioprint

3.1.1. Analytical model without wall slippage

Having discussed the relationships between operational parameters and responses in EBB, mathematical models can be deduced to describe some of these relationships. This can be achieved by performing a force balance in collaboration with the preceding shearing characteristic models described by Eqs. (1)–(3).

To begin developing the mathematical model, consider the steady-state laminar extrusion of a finite elemental bioink filament of radius, r through a cylindrical nozzle of radius, R, and length, L, as illustrated by Fig. (5b), in similarity with the report of Ozbolat [43,147]. The force balance between the prevailing pressures, P, acting on the bioink, bioink's resistance to the flow, i.e., shear stress, τ, and the resulting pressure drop, ΔP, can be expressed by Eq. (8). The pressure drop, ΔP, represents the pressure difference required to initiate the extrusion of bioink.

$$P(\pi r^2) = (P + \Delta P)(\pi r^2) + \tau(2\pi rL) \tag{8}$$

$$\tau = -r\Delta P/2L = r\Delta P/2L \tag{9}$$

Assuming the shearing characteristics of the non-Newtonian bioink follow the Ostwald-de Waele model (without wall slippage), such that Eq. (1) can be substituted into Eq. (9). This substitution leads to Eq. (10), and by rearranging and integrating from the finite elemental bioink radius, r, to the nozzle radius, R, yields the instantaneous extrusion velocity, v, as given in Eq. (11).

$$\int_v^0 dv = -\left(\frac{\Delta P}{2kL}\right)^{1/n} \int_r^R r^{1/n} dr \tag{10}$$

$$v = \left(\frac{n}{n+1}\right)\left(\frac{\Delta P}{2kL}\right)^{1/n}\left(R^{\frac{n+1}{n}} - r^{\frac{n+1}{n}}\right) = \left(\frac{n}{n+1}\right)\left(\frac{\Delta PR}{2kL}\right)^{1/n} R\left(1 - \left(\frac{r}{R}\right)^{\frac{n+1}{n}}\right) \tag{11}$$

By evaluating Eq. (11), the velocity profile for extrusion can be deduced. The maximum extrusion velocity occurs at the core, $r = 0$, and the minimum velocity (i.e., zero) is at the nozzle wall, $r = R$, as illustrated in Fig. (3b). Since the extrusion velocity varies significantly from the core to the wall, it is necessary to calculate the average velocity, $\hat{v}$, through the nozzle. This can be determined from the bioink's instantaneous volumetric flow rate, $q = 2\pi rvdr$, as expressed by Eq. (12), and by integrating results into Eq. (13) [44].

$$\hat{v} = q \Big/ \pi R^2 = 2\pi rvdr \Big/ \pi R^2 = 2 \Big/ R^2 \int_0^R vrdr \tag{12}$$

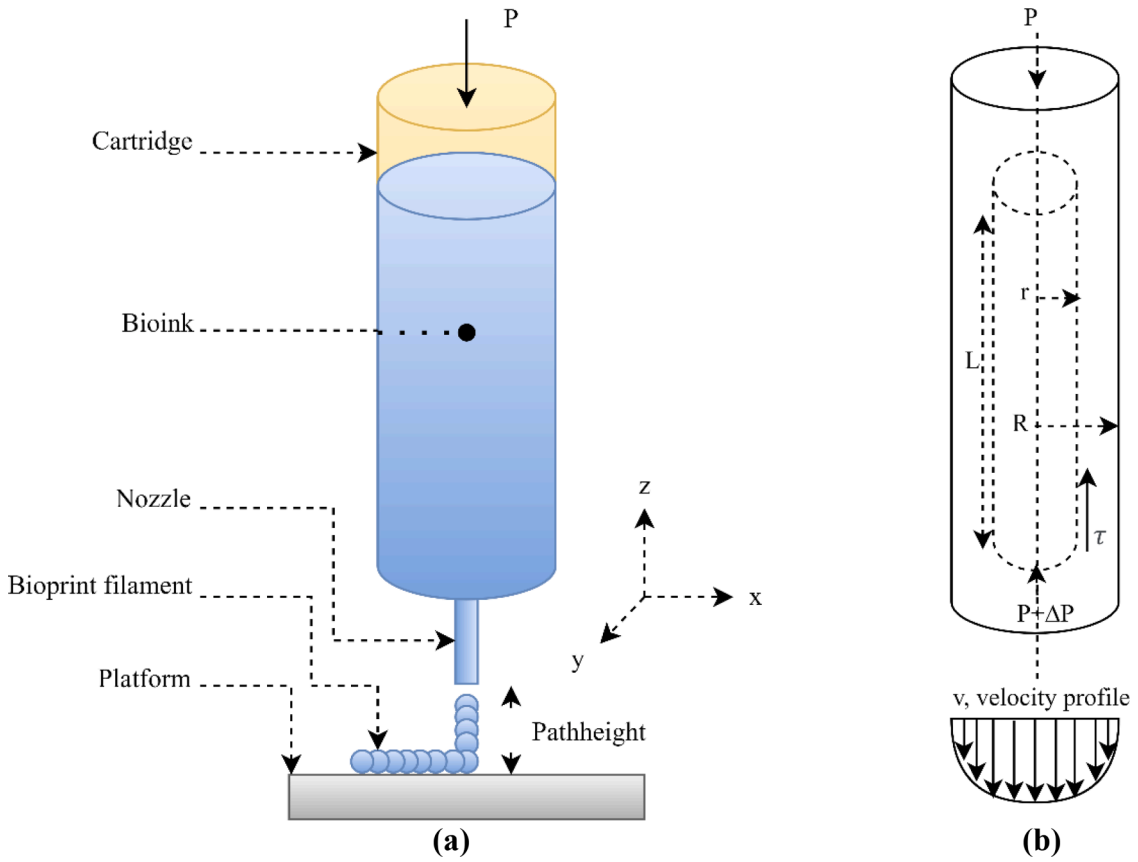

Fig. 5. The flow of bioinks through a cylindrical nozzle of Extrusion-based bioprinting (EBB).

$$\hat{v} = \left(\frac{n}{3n+1}\right)\left(\frac{\Delta P}{2kL}\right)^{1/n} R^{\frac{n+1}{n}} \tag{13}$$

The average velocity, $\hat{v}$ deduced, can be used to estimate the radius of the print filament, R_p, Eq. (15) [148]. This can be achieved through a material balance of the total volumetric flow rate, Q of bioink from the tip of the bioprinter nozzle, R and the volumetric flow rate of the deposited filament on the bioprinter platform, as given by Eq. (14). That means the volumetric flow rate of extrusion is equal to that of deposition, where v_p is the axial velocity [148].

$$\hat{v}\pi R^2 \cong v_p \pi R_p^2 \tag{14}$$

$$R_p \cong R\left(\frac{\hat{v}}{v_p}\right)^{1/2} = \left(\frac{n}{v_p(3n+1)}\right)^{1/2}\left(\frac{\Delta P}{2kL}\right)^{1/2n} R^{\frac{3n+1}{2n}} = f\left(n, k, L, R, \Delta P \;\&\; v_p\right) \tag{15}$$

Nam and Park [149] compared the experimental and analytical flow rates of sodium alginate solution. They examined the extrusion pressure for different nozzle diameters and the filament diameters at different nozzle velocities, using Eq. (15). The analytical and experimental results showed agreement at various nozzle velocities and pressures, up to 32 psi [149].

Preceding the discussion on the relationship of operational parameters with print resolution or shape fidelity, it is important to consider the practical validity of Eq. (15) as demonstrated by Nam and Park [149]. This equation can serve as a measure for correlating and evaluating the relationship between the operational parameters and the print resolution. By mathematically quantifying the bioprint filament radius, R_p (which directly relates to print resolution and consequently shapes fidelity) to the operational parameters. It can be inferred from Eq. (15) that bioprint filament radius, R_p, will always be larger than the nozzle radius, R. Furthermore, the shear-thinning effect has a significant impact on R_p, with a more pronounced effect observed for lower values of the flow behaviour index, n. For instance, when comparing two scenarios with the same bioprinter nozzle radius (R), the R_p at $n = 0.2$ will be greater than the R_p for $n = 0.5$.

In terms of the extrusion pressure, ΔP, an increase in its magnitude will result in a proportional increase in the bioprint filament radius, R_p, with the increment being higher for bioinks exhibiting a more pronounced shear-thinning effect. On the other hand, the flow consistency index, k, and bioprinter nozzle length, L, bioprint filament radius, R_p will decrease by a square root factor of its value, with a more significant decline observed for bioinks with a stronger shear-thinning effect. Similarly, for axial velocity, v_p, an inverse relationship exists with bioprint filament radius, R_p, where higher values of v_p correspond to smaller values R_p, following a square root factor.

Furthermore, the relationship between axial velocity, v_p, and average extrusion velocity, $\hat{v}$, can be deduced from Eq. (14). Similarly, the relationship between v_p and extrusion pressure, ΔP, can be evaluated from Eq. (15). These models clearly demonstrate that extrusion pressure (or velocity) and axial velocity are proportional, which contradicts the claim that extrusion velocity should match axial velocity [139–141]. It supports the claim made by Attalla et al. [139], and other reports [43,147] that the proportionality between extrusion velocity and axial velocity is non-linear. Additionally, Eq. (15) reveals that the flow behaviour index, n, amplifies the effect of all other parameters, suggesting it is a more significant rheological parameter than the flow consistency index, k.

3.1.2. *Analytical model with wall slippage*

It is important to note that the development of Eq. (15) assumes a steady linear shear rate. However, when wall slippage needs to be considered, Eq. (2) can serve as the basis for deriving the instantaneous extrusion velocity, v, average extrusion velocity, $\hat{v}$ and bioprint filament

radius, R_p, as given by Eqs. (16)–(18). Eqs. (16)–(18), can be deduced from the underlying principles used to deduce Eqs. (13)–(15). It is worth mentioning that Eqs. (16)–(18) are unpopular for simulation and comparison with experimental results, even though the assumption on the effect of wall slippage has been highlighted in literature [66,96,112,147–149].

$$v = \left(\frac{n}{n+1}\right)\left(\frac{\Delta PR}{2kL}\right)^{1/n} R\left(1-\left(\frac{r}{R}\right)^{\frac{n+1}{n}}\right) - \left(\frac{\tau_o}{k}\right)^{1/n}(R-r) \tag{16}$$

$$\hat{v} = \left(\frac{n}{3n+1}\right)\left(\frac{\Delta P}{2kL}\right)^{1/n} R^{\frac{n+1}{n}} - \left(\frac{\tau_o}{k}\right)^{1/n} R \Big/ 3 \tag{17}$$

$$R_p = R\left(\frac{\hat{v}}{v_p}\right)^{1/2} = \left(\frac{n}{v_p(3n+1)}\right)^{1/2}\left(\frac{\Delta P}{2kL}\right)^{1/2n} R^{\frac{3n+1}{2n}} - \left(\frac{\tau_o}{k}\right)^{1/2n} R^{3/2} \Big/ 3 = f\left(n, k, \tau_o, L, R, \Delta P \;\&\; v_p\right) \tag{18}$$

In the preceding derivations of Eqs. (8)–(18), the [66,97,113,148–150] mathematical relationships between the operational parameters and bioprint filament radius, R_p, in Eq. (18) are similar to those in Eq. (15). However, the exact mathematical quantification of the effects of the bioprinter nozzle, R, and flow consistency index, k, differs. Specifically, $R_p \propto (\varphi_1 R^{(3n+1)/2n} - \omega_1 R^{3/2})$, and $R_p \propto (\varphi_2 - \omega_2)k^{-1/2n}$. Additionally, the consideration of yield stress, τ_o, is different, where $R_p \propto (\varphi_3 - \omega_3 \tau_o^{-1/2n})$. Note that φ and ω are arbitrary mathematical constants that depend on the specific parameters (i.e., R, k and τ_o) being considered in relation to R_p.

3.1.3. Analytical model based on Poiseuille flow index

Applying an empirical expression (i.e., Poiseuille flow index) for shear rate, $\dot{\gamma}$, Eq. (19) was deduced from an experimental procedure for viscosity measurement. This expression creates the basis for an alternative approach to the derivation of bioprint filament radius, R_p, Eq. (20) and average velocity, $\hat{v}$, Eq. (21) as reported in literature [96,150,151]. Eq. (20) is deduced by the substitution of Eqs. (19) and (9) into Eq. (3), wherein $r = R$. While Eq. (21) is obtained from the substitution of Eq. (20) into Eq. (14). Eqs. (20), (21) were reported to be adequate for identifying the optimal printing parameters to maximise the shape fidelity of bioprint. Moreover, experimental data showed a good agreement with model predictions [96,150,151].

$$\dot{\gamma} = \left(\frac{3n+1}{4n}\right)\frac{4Q}{\pi R^3} = \left(\frac{3n+1}{n}\right)\left(\frac{v_p R_p^2}{R^3}\right) \tag{19}$$

$$R_p = R^2\sqrt{\left(\frac{n}{3n+1}\right)\left(\frac{\Delta P}{2\eta L v_p}\right)} = f\left(n, \eta, L, R, \Delta P \;\&\; v_p\right) \tag{20}$$

$$\hat{v} = v_p\left(\frac{R_p}{R}\right)^2 = \left(\frac{n}{3n+1}\right)\left(\frac{\Delta P R^2}{2\eta L}\right) \tag{21}$$

Eq. (20) differs and its simpler than Eqs. (15) and (18), due to the absence of flow behaviour index, n, as an exponent. Additionally, the effects of flow consistency index, k, and yield stress, τ_o are not accounted for. However, the consideration of the bioink viscosity, η, in this case, incorporates these effects, Eqs. (1)–(3). Another distinction is that the flow behaviour index, n, does not interactively combine with the effect of extrusion pressure, ΔP, nozzle length, L, and radius, R.

3.1.4. Modelling print resolution of EBB bioprint

In summary, the reported models for bioprint filament radius, R_p, Eqs. (15), (18), and (20), have been developed based on specific assumptions. Therefore, the adequacy of these models can only be ascertained via comparison of predicted results to experimental bioprint filament radius, R_{pE} in terms of percentage print resolution, % PR, Eq. (22) as reported by Truccos et al. [151] and as illustrated in Fig. (1c). Note that the closer %PR is to zero the better. An alternative approach reported by Li et al. [112], is to minimise the difference between R_{pE} and R_p via an empirical relationship, $R_{pE} = R_p(1 + C\tau^2)^{1/6}$, that relates them to a fitted shear coefficient, C, and shear stress, τ, using Eq. (15) for R_p. The result of Li et al. [112] report showed adequate proximity between analytical, R_p and experimental, R_{pE}, bioprint filament radius. Although Truccos et al. [151] and Li et al. [112] approaches may be adequate to quantify the difference or even minimise R_p and R_{pE}, they are still limited in their applications. This is because there are some operational parameters such as platform temperature, path-height, path-space, pre-flow and post-flow time whose relationship with bioprint filament radius, R_p can not be analytically described by Eqs. (15), (18), and (20). Alternatively, these parameters can be accounted for by other equations, such as the statistically fitted experimental models, described in the proceeding section.

$$\%PR = \left(\frac{\left|R_{pE} - R_p\right|}{R_p}\right)100 = \left|R_{pE} \Big/ R_p - 1\right|100 \tag{22}$$

The relationship of bioprint filament radius, R_p, to print resolution (%PR), as illustrated in Eq. (22), stems from their definitions and literature review. In 3D bioprinting, print resolution (PR) represents the deposited bioink in the x- and y-direction [50]. In other words, for a given nozzle size, it is a measure of the uniformity of bioink thickness (diameter, $2R_p$) over the smallest unit (a line or arc) of a bioprint filament [152]. The term uniformity implies the absence of contours resulting from swelling or shrinking of the bioprint filament thickness, and length. The length of the bioprint filament is made by the axial movement of the printer head and its thickness by axial velocity, v_p. Eqs. (15), (18), and (20) imply that for a bioink with specific properties, the resulting R_p from given nozzle sizes significantly influences PR [153]. Furthermore, because PR in collaboration with dimensionality (print resolution in the z-direction, i.e., the uniformity of the height of layered bioprint filaments) constitute shape fidelity [50], it means that better PR result in better shape fidelity.

3.2. Modelling cell viability in EBB bioprint

While several experimental models have been reported in the literature to describe cell viability during bioprinting [74,148,154], a theoretical model derived from established physical principles for cell viability in relation to shear stress and other factors has not been developed. Lemarie et al. [154] reported a linear model, based on the linear portion of the generalised statistical model, Eq. (23). This model describes cell viability (i.e., $f_i(x) = \%CV$) for different nozzle geometry and diameter via correlation with three parameters (i.e., $\mathscr{K} = 3$): wall shear stress, $\tau = x_1$; residence time, $t = x_2$; and bioink viscosity, $\eta = x_3$, using actual experimental values, ξ, instead of coded values (x). Ning et al. [148], on the other hand, presented an exponential model, Eq. (24), based on observed parabolic trends exhibited by cell death. This approach is more realistic than a linear model that assumes an accelerated cell death without plateauing. Where b_o, b_1, and b_2 are experimentally curve-fitted factors. Nair et al. [74], however, developed a more comprehensive statistical model for cell viability (i.e. $f_i(x) = \%CV$) that accounts for all components of Eq. (23) in correlation with two parameters (i.e. $\mathscr{K} = 2$): extrusion pressure, $\Delta P = x_1$; and nozzle diameter, $2R = x_2$ in terms of coded experimental values, x. The model proposed by Nair et al. [74] is more robust as it incorporates quadratic, interactive, and linear terms, addressing the limitations of the linear model assumption and accounting for the plateauing effect observed in the exponential model. In Eq. (23), x_i and x_j represent independent parameters, β_o is a constant of the independent variables, β_i is the linear term coefficient, β_{ii} is the quadratic term coefficient, β_{ij} is the cross-term or interactive coefficient, and $\mathscr{K}$ is the number of parameters considered.

$$f(x) = \beta_o + \sum_{i=1}^{\mathscr{K}} \beta_i x_i + \sum_{i=1}^{\mathscr{K}} \beta_{ii} x_i^2 + \sum_{i=1}^{\mathscr{K}} \sum_{j=1}^{\mathscr{K}} \beta_{ij} x_i x_j \quad (23)$$

$$\%CV = 100\left[1 - \exp\left(-b_o \tau^{b_1} t^{b_2}\right)\right] \quad (24)$$

Eq. (23) is typically developed by considering statistically significant parameters with a probability value of less than 5% (i.e., P-value < 0.05) or 95% confidence interval fence [74]. Therefore, it can be generally applied to any process based on the statistical significance of experimental results between the investigated parameters, x, and the corresponding expected results or responses, $f_i(x)$. On this premise, Eq. (23) can also be applied to model the bioprint filament radius, R_p, especially when investigating its dependence on operational parameters like platform temperature, path-height, path-space, pre-flow and post-flow time.

3.2.1. Statistical model development

A reliable approach for developing the statistical or multivariable regression model highlighted in Eq. (23) is through classical Design of Experiment (DOE), which employs various methodologies such as factorial design, response surface methodology (e.g., Central Composite Design [CCD], Box-Behnken Design [BBD]), and others [155]. These methodologies serve as precursors for optimising the deduced responses, $f_i(x)$. In DOE, a specific number of experimental runs, Eq. (25) are performed, depending on the number of parameters, $\mathscr{K}$, as well as the number of centre points, $\varkappa_c$, considered. Additionally, DOE typically utilises coded values, x, to express the operational parameters rather than their actual experimental values, ξ. The relationship between coded values, x, and actual experimental values, ξ, is defined by Eq. (26).

$$N = \mathscr{K}^2 + 2\mathscr{K} + \varkappa_c \quad (25)$$

$$x = \frac{(\xi - \overline{\xi})}{\beta \xi_{Range}} \quad (26)$$

$$\beta = \frac{(\xi_{max} - \overline{\xi})}{\alpha \xi_{Range}} \quad (27a)$$

$$\beta = \frac{(\xi_{max} - \overline{\xi})}{\xi_{Range}} \quad (27b)$$

Where, $\xi_{Range} = (\xi_{max} - \xi_{min})$, is the actual value range (i.e., the difference between the maximum, ξ_{max} and minimum, ξ_{min} value), $\overline{\xi} = 0.5(\xi_{max} + \xi_{min})$, is the actual average value and β, is a constant specific to the type of DOE. Typically for CCD design, β is given by Eq. (27a) or (27b) depending on the allowable upper and lower limit of the actual values of parameters in the process being considered. Where the 'star points' that allow for evaluation of curvature are given by $\alpha = \pm(2^k)^{\pm 0.25}$ [156]. Each process parameter used in the CCD is distributed over the limits illustrated in Table (5): upper limit, $+\alpha$; upper mid-point, $+1$; mid-point, 0; lower mid-point, -1; lower limit, $-\alpha$ for circumscribed CCD.

4. Optimisation of shape fidelity and cell viability during bioprinting

Having discussed the models representing bioprinting responses (print resolution, %PR, and cell viability, %CV) to printing parameters (extrusion pressure or velocity, nozzle geometry, nozzle diameter; cartridge temperature, platform temperature, axial velocity, pre-flow time, post-flow time, path-height, and path-space time), these models can be used for bioprinting optimisation. Table (6) summarises the application, advantages and disadvantages of these models. Considering that some parameters interact with each other and that the two responses (print resolution and cell viability) are in competition due to shear stress, a multivariable-multiobjective optimisation approach for EBB can be proposed. This optimisation approach shares similarities with the approach applied by Shi et al.[157] for optimising shape fidelity, and satellite formation for drop-on-demand bioprinting. However, it is

Table 6
Summary of reported models applicable for print resolution and cell viability.

Model purpose	Model	Advantages	Disadvantages
Bioprint filament radius [43, 147,149]	Eq. (15)	Report analytical relationship with extrusion pressure, or velocity, axial velocity, nozzle size, and cartridge temperature (via Arrhenius equation); Lesser parameters, as such cheap and take less time to develop	Complex analytical relationships with parameters; Neglect the effect of wall slippage, and other bioprinting parameters such as platform temperature, pre-flow time, and post-flow time
Bioprint filament radius [66, 96,112, 147–149]	Eq. (18)	Report analytical relationship with extrusion pressure, or velocity, axial velocity, nozzle size, cartridge temperature (via Arrhenius equation), as well as wall slippage via yield stress; Lesser parameters, as such cheap and take less time to develop	Complex analytical relationships with parameters; Neglect the other bioprinting parameters
Bioprint filament radius [96, 150,151]	Eq. (20)	Simplified analytical relationship with extrusion pressure, or velocity, axial velocity, nozzle size, cartridge temperature (via Arrhenius equation); Lesser parameters, as such cheap and take less time to develop	Neglect the effect of wall slippage, flow consistency index, and other bioprinting parameters
Cell viability [74,154]	Eq. (23)	Simplified statistical model with the ability to incorporate all statistically significant bioprinting parameters.	Depending on the number of parameters to consider, it maybe expensive and take a lot of time to develop
Cell viability [148]	Eq. (24)	Simplified curve-fitted relationship with wall shear stress and residence time; Cheap and less time to develop	Does not consider the effect of other bioprinting parameters

Table 5
Illustration of coded and actual limits of parameters for inscribed central composite design.

Variable, unit	symbols	Coded and actual value				
		x_i(-1), lower limits	x_i(-α), Lower midpoints	x_i(0), midpoints	x_i(+α), Upper midpoints	x_i(1), upper limits
Extrusion pressure, Pa	ξ_1	$\varepsilon_{-1,1}$	$\varepsilon_{-\alpha,1}$	$\varepsilon_{0,1}$	$\varepsilon_{-1,1}$	$\varepsilon_{-\alpha,1}$
⋮	⋮	⋮	⋮	⋮	⋮	⋮
Platform temperature, °C	$\xi_{\mathscr{K}}$	$\varepsilon_{-1,\mathscr{K}}$	$\varepsilon_{-\alpha,\mathscr{K}}$	$\varepsilon_{0,\mathscr{K}}$	$\varepsilon_{-1,\mathscr{K}}$	$\varepsilon_{-\alpha,\mathscr{K}}$

worth noting that most studies on the optimisation of bioprinting shape fidelity and cell viability have typically followed factor-by-factor and single-objective optimisation routes [47,74–76]. For instance, Webb and Doyle [47] and Lewicki et al. [75] employed a so-called Printing Optimisation Index (POI) to simultaneously optimise the shape fidelity and cell viability of hydrogel.

Successful optimisation of bioprinting necessitates knowledge of the acceptable limits of bioprinting parameters, which has been thoroughly reviewed by Sánchez et al. [69]. In summary, the following reasonable minimum and maximum value range for cell-laden bioink were proposed: (15,40)°C for cartridge temperature; (0,40)°C for platform temperature; (5×10^{-6},10) bar for extrusion pressure; (210,514) μm for nozzle diameter and (0.2,400) $mm.s^{-1}$ for axial velocity. However, it is important to note that these reported ranges might be constrained by the allowable limits of the available bioprinters and associated accessories.

4.1. Proposition for multivariable-multiobjective optimisation

On the premise of using Eq. (23) for cell viability prediction due to earlier stated reasons, and using either Eqs. (15), (18), (20), or (23) for bioprint filament radius in conjunction with percentage print resolution (%PR), Eq. (22), the bioprinting process can be optimised. Depending on how rigorous the bioprinting optimisation is intended (i.e., considering the number of parameters), two propositions can be explored using the general multivariable-multiobjective optimisation structure, Eq. (28) [158]. Where %PR is intended to be minimised, %CV is to be maximised (i.e., minimise $-$ %CV); G(x) denotes the vector of non-linear inequality constraint; H(x) represents the vector of non-linear equality constraint; g represents the coefficients of parameters in the linear inequality constraint; s is the constants in the linear inequality constraint; h represents the coefficient of parameters in the linear equality constraint; and m represents the constant for linear equality constraint. The constraint models are formulated based on the operational parameters, x, with lower limits, l, and upper limit, u. Note that when using Eq. (23) in collaboration with Eqs. (15), (18), or (20) for optimisation purposes, then parameters in Eq. (23) must be expressed in terms of their actual values, ξ (i.e., $x = \xi$). Among other software options, Eq. (28) can be solved in MATLAB using multi-objective optimisation functions such as fminimax and gamultiobj [159].

$$\text{minimise}\{\%PR(x), -\%CV(x)\} \tag{28}$$

Subject to

$$\text{Inequality constraint} \begin{cases} G(x) \le 0 \\ gx \le s \end{cases}$$

$$\text{Equality constraint} \begin{cases} H(x) = 0 \\ hx = m \end{cases}$$

Allowable limits $l \le x \le u$

Proposition 1

Assuming prior knowledge of certain bioprinting parameters are known, and/or resources are limited in the number of experiments that can be performed. Specifically, assuming values of parameters such as nozzle geometry, platform temperature, pre-flow time, post-flow time, path-height and path-space are fixed or their optimal already known, and that the optimal values of parameters such as extrusion pressure, ΔP or velocity, $\hat{v}$, axial velocity, v_p, nozzle size, R and cartridge temperature, T_c that minimises percentage print resolution %PR(x) = f (ΔP, v_p, R and T_c), as well as maximises percentage cell viability, %CV(x) = f (ΔP, v_p, R and T_c) are to be determined (i.e., four parameters, $\mathscr{K} = 4$, hence requiring a minimum experiment of N = 24). Then Eq. (28) can be solved to determine these optimal values, using Eqs. (15), (18), or (20) to obtain R_p in %PR(x), Eqs. (22), and (23) to calculate %CV(x). Note that cartridge temperature can be incorporated into R_p in %PR via its influence on the bioink flow consistency index, k, flow behaviour index, n, yield stress, τ_o and apparent viscosity, η as highlighted by Eqs. (4)–(6). In summary, this proposition leverages analytical models, Eqs. (15), (18), or (20) in collaboration with experimental statistically fitted models, Eq. (23). Since the number of parameters to optimise is limited due to the number of parameters in the analytical model, the number of experiments to perform will also be limited.

Consider an example illustration of Eq. (28) based on this proposition outlined in Eq. (29). In this illustration, Eq. (20) was used for the estimation of R_p, in Eq. (22), and augmented with Eq. (4) to account for the influence of T_c. Additionally, Eq. (23) is used to model cell viability in terms of actual experimental values, ξ (ΔP, v_p, R and T_c). The bioprinting process is assumed to be subject to lower (0.5 bar, 0.8 $mm.s^{-1}$, 0.1 mm, 4.0 °C) and upper (1.5 bar, 100 $mm.s^{-1}$, 0.42 mm, 40 °C) limits.

$$\text{minimise}\begin{cases} \left| R_{pE} \Big/ R^2\sqrt{(n/(3n+1))(\Delta P/2\eta L v_p)} - 1 \right| 100 \\ -\left(\beta_o + \beta_1\Delta P + .. + \beta_4 T_c + \beta_{11}\Delta P^2 + .. + \beta_{44}T_c^2 + \beta_{12}\Delta P.v_p + .. + \beta_{14}\Delta P.T_c\right) \end{cases} \tag{29}$$

$$n, \eta = A_0 \exp(E_a / RT_c)$$

Subject to

$$0.5 \le \Delta P \le 1.5 bar$$

$$0.8 \le v_P \le 100 mm.s^{-1}$$

$$0.1 \le R \le 0.42 mm$$

$$4.0 \le T_C \le 40^{\circ}C$$

Note that while the percentage print resolution (%PR), Eq. (22), is deduced through R_p analytically derived as given by Eq. (20) in Section (3.1). The percentage cell viability (%CV) is derived by multivariable regression described in Section (3.2.1).

Proposition 2

In the case where a comprehensive investigation of optimal values of bioprinting parameters is required, such that more parameters: extrusion pressure, ΔP or velocity, $\hat{v}$, axial velocity, v_p, nozzle size, R, cartridge temperature, T_c, platform temperature, T_p, pre-flow time, t_{pe}, post-flow time, t_p, path-height, h_h, and path-space, h_s (i.e. nine parameters, $\mathscr{K} = 9$, hence requiring a minimum experiment of N = 99) are to be considered. As earlier discussed, in this case, Eq. (23) will be the choice in modelling both R_p in percentage print resolution %PR(x) = f (ΔP, v_p, R, T_c, T_p, t_{pe}, t_p, h_h and h_s), and percentage cell viability, %CV(x) = f (ΔP, v_p, R, T_c, T_p, t_{pe}, t_p, h_h and h_s) in the optimisation model, Eq. (28). Contrary to Proposition 1, the cartridge temperature can be directly incorporated into R_p for the %PR model, like other parameters.

Similarly in the case of Proposition 2, the optimisation model can be represented by Eq. (30), specifically using the coded values, x_i, of the parameters. The subscript, i = 1, 2,…, $\mathscr{K}$ represents the parameters ΔP, v_p, R, T_c, T_p, t_{pe}, t_p, h_h and h_s. Where in this case β' typically depicts the constant and coefficients of the PR model, analogous to β in Eq. (23)

used for the CV model.

$$\text{minimise}\begin{cases} \beta_o^{'}+\beta_1^{'}x_1+..+\beta_9^{'}x_9+\beta_{11}^{'}x_1^2+..+\beta_{99}^{'}x_9^2+\beta_{12}^{'}x_1x_2+..+\beta_{19}^{'}x_1x_9 \\ -\left(\beta_o+\beta_1x_1+..+\beta_9x_9+\beta_{11}x_1^2+..+\beta_{99}x_9^2+\beta_{12}x_1x_2+..+\beta_{19}x_1x_9\right) \end{cases} \quad (30)$$

Subject to

$$-1 \le x_i \le 1$$

Note that both percentage print resolution (%PR), Eq. (22), is deduced through R_p derived by multivariable regression, as well as the percentage cell viability (%CV) described in Section (3.2.1).

In evaluating the two propositions, Proposition 2 offers a more rigorous, and accurate approach compared to Proposition 1. However, Proposition 2 requires a larger number of experimental runs, making it potentially more expensive and time-consuming than Proposition 1. Proposition 2 is particularly suitable for modelling parameters that do not have a known analytical relationship with bioprint responses. Typically, parameters such as pre-flow time, post-flow time, path-height, and path-space can be modelled into R_p in percentage print resolution %PR(x) since these parameters have been reported to influence print resolution or shape fidelity [139–141]). Similarly, as high platform temperature is known to hurt living cells [69]).

4.2. Summarised applicability of propositions

In summary Proposition 1 offers a simplified approach when prior knowledge is available regarding optimal values that specifically enhance print resolution or shape fidelity for familiar shapes and/or bioinks. Consider a situation where it is required to reprint a construct with a different type of bioink. Furthermore, assuming in the previous work the optimal platform temperature, pre-flow time, post-flow time, path-height and path-space (if they were significant or had an adequate correlation to the responses) have been deduced via Proposition 2. It will be appropriate to perform the optimisation of the task with the new bioink through Proposition 1 rather than with Proposition 2. This is because only the rheology of the process (i.e. bioink) has changed, as such it is expected to affect the shear stress of the process. And since there is no logical correlation between bioink rheology as well shear stress to platform temperature, pre-flow time, post-flow time, path-height and path-space; as opposed to extrusion pressure, ΔP or velocity, $\hat{v}$, axial velocity, v_p, nozzle size, R (applicable only if a different nozzle is to be applied), cartridge temperature, T_c. Furthermore, in another situation where a different shape is to be printed, however with a known type of bioink, hence its rheological properties are also known. It will also be appropriate to apply Proposition 1 rather than Proposition 2. This is because it is likely that it would only be necessary to optimise; platform temperature, pre-flow time, post-flow time, path-height and path-space depending on their significance to the response. In this case, it should be however noted that Eq. (23) will be the choice in modelling both R_p in percentage print resolution %PR(x) and percentage cell viability, %CV(x) in the optimisation model, Eq. (28) in a similar fashion illustrated in Proposition 2. Although with a reduced number of experiments (i.e., four parameters, $\mathscr{K} = 5$, hence requiring a minimum experiment of $N = 35$).

On the other hand, Proposition 2 is best applied during the initial developmental stage of bioprinting for new shapes and bioinks, where a more comprehensive exploration of parameters is necessary. Furthermore, even though machine learning is not the focus of this study, however as time progresses (i.e., over the years) sufficient data is likely to be generated from Proposition 1 and Proposition 2 that could be subsequently applied for machine learning development. Therefore mathematical modelling and optimisation through the highlighted propositions can serve as a precursor to machine learning applications, as highlighted in Table (7).

Table 7
Summarised comparisons of Proposition 1 and Proposition 2.

Consideration	Proposition 1	Proposition 2
Initial product development	Not suitable	More suitable
Development of familiar shape with new bioink	Suitable	Not suitable
Development of new shape with familiar bioink	Suitable	Not suitable
Applicable models	All model types	Statistical model
Experimental runs and resources	Limited as such less expensive	Higher as such more expensive
Machine learning application	Applicable over time	Applicable over time

5. Conclusion

In conclusion, two propositions have been suggested for the effective optimisation of extrusion-based bioprinting (EBB). These propositions were based on multivariable-multiobjective optimisations, taking into account multiple operational parameters or variables (extrusion pressure or velocity, nozzle geometry, nozzle diameter; cartridge temperature, platform temperature, axial velocity, pre-flow time, post-flow time, path-height, and path-space time) and the competing influences of shear stress on the bioprinting responses or objectives: Print resolution, PR or shape fidelity and cell viability, CV. It was reported that Proposition 1 offers a simplified approach when prior knowledge of optimal parameter values that specifically influence shape fidelity is available for familiar bioinks and bioprint shapes. While Proposition 2, a more rigorous approach, is suitable for the initial developmental stage of bioprinting new bioprint shapes with new bioinks.

To lay a robust foundation for these propositions, a thorough review of bioink shearing characteristics and models describing extrusion-based bioprinting was conducted. It was found that bioink shearing characteristics are predominantly shear-thinning and can be described by models such as the Ostwald-de Waele model, as well as the Herschel-Bulkley model, among other reported models. The study also discussed how temperature and time dependence can be incorporated into the modelling of bioink's shearing characteristics using rheological parameters such as flow consistency index, k, flow behaviour index, n, shear stress, τ, yield stress, τ_o, and apparent viscosity, η and in collaboration with the Arrhenius model, as well as other forms of models. Theoretical and experimental models from literature that are useful for modelling EBB were highlighted, specifically focusing on models for bioprint filament radius, R_p, and cell viability, CV. These models were evaluated based on rheology, the incorporation of bioprinting parameters, and their mathematical relationships.

In light of these evaluations and following the structure of multivariable-multiobjective optimisation, the two propositions were developed. It is expected that in future studies, these propositions will be further explored and applied in the bioprinting of hyaluronic acid-based bioinks.

Declaration of Competing Interest

The authors declare that they have no known competing financial interests or personal relationships that could have appeared to influence the work reported in this paper.

Data availability

No data was used for the research described in the article.

Acknowledgement

The research was funded by Tomas Bata University, Zlin, Czech Republic through the project OP RDE Junior Grants, Reg. No.

CZ.02.2.69/0.0/0.0/19_073/0016941.

References

[1] J. Yu, S.A. Park, W.D. Kim, T. Ha, Y.Z. Xin, J. Lee, et al., Current advances in 3D bioprinting technology and its applications for tissue engineering, Polymers 12 (2020) 1–30, https://doi.org/10.3390/POLYM12122958 (Basel).

[2] B. Zhang, L. Gao, L. Ma, Y. Luo, H. Yang, Z. Cui, 3D bioprinting: a novel avenue for manufacturing tissues and organs, Engineering 5 (2019) 777–794, https://doi.org/10.1016/J.ENG.2019.03.009.

[3] I.T. Ozbolat, K.K. Moncal, H. Gudapati, Evaluation of bioprinter technologies, Addit. Manuf. 13 (2017) 179–200, https://doi.org/10.1016/J.ADDMA.2016.10.003.

[4] R.J. Klebe, Cytoscribing: a method for micropositioning cells and the construction of two- and three-dimensional synthetic tissues, Exp. Cell Res. 179 (1988) 362–373, https://doi.org/10.1016/0014-4827(88)90275-3.

[5] S. Ji, M. Guvendiren, Recent advances in bioink design for 3D bioprinting of tissues and organs, Front. Bioeng. Biotechnol. 5 (2017), https://doi.org/10.3389/FBIOE.2017.00023.

[6] P.K. Chandra, S. Soker, A. Atala, Tissue engineering: current status and future perspectives, Princ. Tissue Eng. (2020) 1–35, https://doi.org/10.1016/B978-0-12-818422-6.00004-6.

[7] J. Adhikari, A. Roy, A. Das, M. Ghosh, S. Thomas, A. Sinha, et al., Effects of processing parameters of 3D bioprinting on the cellular activity of bioinks, Macromol. Biosci. 21 (2021), 2000179, https://doi.org/10.1002/MABI.202000179.

[8] Biazar E., Najafi S.M., Heidari K.S., Yazdankhah M., Rafiei A., Biazar D. 3D bioprinting technology for body tissues and organs regeneration. 2018;42:187–202. doi:10.1080/03091902.2018.1457094.

[9] E.S. Bishop, S. Mostafa, M. Pakvasa, H.H. Luu, M.J. Lee, J.M. Wolf, et al., 3-D bioprinting technologies in tissue engineering and regenerative medicine: current and future trends, Genes Dis. 4 (2017) 185–195, https://doi.org/10.1016/J.GENDIS.2017.10.002.

[10] M.D. Sarker, S. Naghieh, N.K. Sharma, L. Ning, X. Chen, Bioprinting of vascularized tissue scaffolds: influence of biopolymer, cells, growth factors, and gene delivery, J. Healthc. Eng. 2019 (2019), https://doi.org/10.1155/2019/9156921.

[11] L. Ning, N. Zhu, A. Smith, A. Rajaram, H. Hou, S. Srinivasan, et al., Noninvasive three-dimensional *in situ* and *in vivo* characterization of bioprinted hydrogel scaffolds using the X-ray propagation-based imaging technique, ACS Appl. Mater. Interfaces 13 (2021) 25611–25623, https://doi.org/10.1021/ACSAMI.1C02297.

[12] B. Schmieg, S. Gretzinger, S. Schuhmann, G. Guthausen, J. Hubbuch, Magnetic resonance imaging as a tool for quality control in extrusion-based bioprinting, Biotechnol. J. 17 (2022), 2100336, https://doi.org/10.1002/BIOT.202100336.

[13] I.F. Cengiz, M. Pitikakis, L. Cesario, P. Parascandolo, L. Vosilla, G. Viano, et al., Building the basis for patient-specific meniscal scaffolds: from human knee MRI to fabrication of 3D printed scaffolds, Bioprinting (2016) 1–2, https://doi.org/10.1016/J.BPRINT.2016.05.001, 1–10.

[14] A. Ruland, K.J. Gilmore, L.Y. Daikuara, C.D. Fay, Z. Yue, G.G. Wallace, Quantitative ultrasound imaging of cell-laden hydrogels and printed constructs, Acta Biomater. 91 (2019) 173–185, https://doi.org/10.1016/J.ACTBIO.2019.04.055.

[15] S. Yang, L. Wang, Q. Chen, M. Xu, *In situ* process monitoring and automated multi-parameter evaluation using optical coherence tomography during extrusion-based bioprinting, Addit. Manuf. 47 (2021), 102251, https://doi.org/10.1016/J.ADDMA.2021.102251.

[16] N. Hong, G.H. Yang, J.H. Lee, G.H. Kim, 3D bioprinting and its *in vivo* applications, J. Biomed. Mater. Res. B Appl. Biomater. 106 (2018) 444–459, https://doi.org/10.1002/JBM.B.33826.

[17] Thomas D.J. 3D printing techniques in medicine and surgery. 3D printing in medicine and surgery: applications in healthcare 2021:15–45. doi:10.1016/B978-0-08-102542-0.00003-8.

[18] D.F.D. Campos, M.A. Philip, S. Gürzing, C. Melcher, Y.Y. Lin, J. Schöneberg, et al., Synchronized dual bioprinting of bioinks and biomaterial inks as a translational strategy for cartilage tissue engineering, 3D Print. Addit. Manuf. 6 (2019) 63–71, https://doi.org/10.1089/3DP.2018.0123.

[19] A. Schwab, R. Levato, M. D'Este, S. Piluso, D. Eglin, J. Malda, Printability and shape fidelity of bioinks in 3D bioprinting, Chem. Rev. 120 (2020) 11028–11055, https://doi.org/10.1021/ACS.CHEMREV.0C00084.

[20] J. Groll, J.A. Burdick, D.W. Cho, B. Derby, M. Gelinsky, S.C. Heilshorn, et al., A definition of bioinks and their distinction from biomaterial inks, Biofabrication 11 (2018), https://doi.org/10.1088/1758-5090/AAEC52.

[21] P. Wang, Y. Sun, X. Shi, H. Shen, H. Ning, H. Liu, 3D printing of tissue engineering scaffolds: a focus on vascular regeneration, Bio-Des. Manuf. 4 (2021) 344–378, https://doi.org/10.1007/S42242-020-00109-0, 2021 4:2.

[22] P.S. Gungor-Ozkerim, I. Inci, Y.S. Zhang, A. Khademhosseini, M.R. Dokmeci, Bioinks for 3D bioprinting: an overview, Biomater. Sci. 6 (2018) 915–946, https://doi.org/10.1039/C7BM00765E.

[23] H. Li, C. Tan, L. Li, Review of 3D printable hydrogels and constructs, Mater. Des. 159 (2018) 20–38, https://doi.org/10.1016/J.MATDES.2018.08.023.

[24] J. Gopinathan, I. Noh, Recent trends in bioinks for 3D printing, Biomater. Res. 22 (2018) 1–15, https://doi.org/10.1186/S40824-018-0122-1, 2018 22:1.

[25] M. Hospodiuk, M. Dey, D. Sosnoski, I.T. Ozbolat, The bioink: a comprehensive review on bioprintable materials, Biotechnol. Adv. 35 (2017) 217–239, https://doi.org/10.1016/J.BIOTECHADV.2016.12.006.

[26] W. Zhao, X. Jin, Y. Cong, Y. Liu, J. Fu, Degradable natural polymer hydrogels for articular cartilage tissue engineering, J. Chem. Technol. Biotechnol. 88 (2013) 327–339, https://doi.org/10.1002/JCTB.3970.

[27] S. Kapoor, S.C. Kundu, Silk protein-based hydrogels: promising advanced materials for biomedical applications, Acta Biomater. 31 (2016) 17–32, https://doi.org/10.1016/J.ACTBIO.2015.11.034.

[28] F.P.W. Melchels, M.A.N. Domingos, T.J. Klein, J. Malda, P.J. Bartolo, D. W. Hutmacher, Additive manufacturing of tissues and organs, Prog. Polym. Sci. 37 (2012) 1079–1104, https://doi.org/10.1016/J.PROGPOLYMSCI.2011.11.007.

[29] E.S. Place, J.H. George, C.K. Williams, M.M. Stevens, Synthetic polymer scaffolds for tissue engineering, Chem. Soc. Rev. 38 (2009) 1139–1151, https://doi.org/10.1039/B811392K.

[30] M.S.B. Reddy, D. Ponnamma, R. Choudhary, K.K. Sadasivuni, A comparative review of natural and synthetic biopolymer composite scaffolds, Polymers 13 (2021) 1105, https://doi.org/10.3390/POLYM13071105, 13Page 1105-2021.

[31] K. Markstedt, A. Mantas, I. Tournier, H. Martínez Ávila, D. Hägg, P. Gatenholm, 3D bioprinting human chondrocytes with nanocellulose-alginate bioink for cartilage tissue engineering applications, Biomacromolecules 16 (2015) 1489–1496, https://doi.org/10.1021/ACS.BIOMAC.5B00188.

[32] R. Ramakrishnan, N. Kasoju, R. Raju, R. Geevarghese, A. Gauthaman, A. Bhatt, Exploring the potential of alginate-gelatin-diethylaminoethyl cellulose-fibrinogen based bioink for 3D bioprinting of skin tissue constructs, Carbohydr. Polym. Technol. Appl. 3 (2022), 100184, https://doi.org/10.1016/J.CARPTA.2022.100184.

[33] Y. Yang, R. Xu, C. Wang, Y. Guo, W. Sun, L. Ouyang, Recombinant human collagen-based bioinks for the 3D bioprinting of full-thickness human skin equivalent, Int. J. Bioprint. 8 (2022) 145–160, https://doi.org/10.18063/IJB.V8I4.611.

[34] M. Zhao, J. Wang, J. Zhang, J. Huang, L. Luo, Y. Yang, et al., Functionalizing multi-component bioink with platelet-rich plasma for customized *in-situ* bilayer bioprinting for wound healing, Mater. Today Bio 16 (2022), https://doi.org/10.1016/J.MTBIO.2022.100334.

[35] Y.W. Ding, X.W. Zhang, C.H. Mi, X.Y. Qi, J. Zhou, D.X. Wei, Recent advances in hyaluronic acid-based hydrogels for 3D bioprinting in tissue engineering applications, Smart Mater. Med. 4 (2023) 59–68, https://doi.org/10.1016/J.SMAIM.2022.07.003.

[36] S.K. Schmidt, R. Schmid, A. Arkudas, A. Kengelbach-Weigand, A.K. Bosserhoff, Tumor cells develop defined cellular phenotypes after 3D-bioprinting in different bioinks, Cells 8 (2019) 1295, https://doi.org/10.3390/CELLS8101295. Page 1295-20198.

[37] S. Coşkun, S.O. Akbulut, B. Sarıkaya, S. Çakmak, M. Gümüşderelioğlu, Formulation of chitosan and chitosan-nanoHAp bioinks and investigation of printability with optimized bioprinting parameters, Int. J. Biol. Macromol. 222 (2022) 1453–1464, https://doi.org/10.1016/J.IJBIOMAC.2022.09.078.

[38] X. Liu, B. Gaihre, M.N. George, A.L. Miller, H. Xu, B.E. Waletzki, et al., 3D bioprinting of oligo(poly[ethylene glycol] fumarate) for bone and nerve tissue engineering, J. Biomed. Mater. Res. A 109 (2021) 6–17, https://doi.org/10.1002/JBM.A.37002.

[39] M. Nowicki, W. Zhu, K. Sarkar, R. Rao, L.G. Zhang, 3D printing multiphasic osteochondral tissue constructs with nano to micro features via PCL based bioink, Bioprinting 17 (2020) e00066, https://doi.org/10.1016/J.BPRINT.2019.E00066.

[40] K.C.R. Kolan, J.A. Semon, A.T. Bindbeutel, D.E. Day, M.C. Leu, Bioprinting with bioactive glass loaded polylactic acid composite and human adipose stem cells, Bioprinting 18 (2020) e00075, https://doi.org/10.1016/J.BPRINT.2020.E00075.

[41] G. Choe, M. Lee, S. Oh, J.M. Seok, J. Kim, S. Im, et al., Three-dimensional bioprinting of mesenchymal stem cells using an osteoinductive bioink containing alginate and BMP-2-loaded PLGA nanoparticles for bone tissue engineering, Biomater. Adv. 136 (2022), 212789, https://doi.org/10.1016/J.BIOADV.2022.212789.

[42] J.M. Seok, S.H. Oh, S.J. Lee, J.H. Lee, W.D. Kim, S.H. Park, et al., Fabrication and characterization of 3D scaffolds made from blends of sodium alginate and poly (vinyl alcohol), Mater. Today Commun. 19 (2019) 56–61, https://doi.org/10.1016/J.MTCOMM.2018.09.013.

[43] A.S. Theus, L. Ning, B. Hwang, C. Gil, S. Chen, A. Wombwell, et al., Bioprintability: physiomechanical and biological requirements of materials for 3D bioprinting processes, Polymers 12 (2020) 1–19, https://doi.org/10.3390/POLYM12102262 (Basel).

[44] N. Paxton, W. Smolan, T. Böck, F. Melchels, J. Groll, T. Jungst, Proposal to assess printability of bioinks for extrusion-based bioprinting and evaluation of rheological properties governing bioprintability, Biofabrication 9 (2017), https://doi.org/10.1088/1758-5090/AA8DD8.

[45] T. Ahlfeld, V. Guduric, S. Duin, A.R. Akkineni, K. Schütz, D. Kilian, et al., Methylcellulose – a versatile printing material that enables biofabrication of tissue equivalents with high shape fidelity, Biomater. Sci. 8 (2020) 2102–2110, https://doi.org/10.1039/D0BM00027B.

[46] S. Ramesh, O.L.A. Harrysson, P.K. Rao, A. Tamayol, D.R. Cormier, Y. Zhang, et al., Extrusion bioprinting: recent progress, challenges, and future opportunities, Bioprinting 21 (2021) e00116, https://doi.org/10.1016/J.BPRINT.2020.E00116.

[47] B. Webb, B.J. Doyle, Parameter optimization for 3D bioprinting of hydrogels, Bioprinting 8 (2017) 8–12, https://doi.org/10.1016/J.BPRINT.2017.09.001.

[48] L. Hahn, E. Karakaya, T. Zorn, B. Sochor, M. Maier, P. Stahlhut, et al., An inverse thermogelling bioink based on an ABA-type poly(2-oxazoline) amphiphile, Biomacromolecules 22 (2021) 3017–3027, https://doi.org/10.1021/ACS.BIOMAC.1C00427.

[49] A. Ribeiro, M.M. Blokzijl, R. Levato, C.W. Visser, M. Castilho, W.E. Hennink, et al., Assessing bioink shape fidelity to aid material development in 3D bioprinting, Biofabrication 10 (2018), https://doi.org/10.1088/1758-5090/AA90E2.
[50] J.M. Lee, W.L. Ng, W.Y. Yeong, Resolution and shape in bioprinting: strategizing towards complex tissue and organ printing, Appl. Phys. Rev. 6 (2019), https://doi.org/10.1063/1.5053909.
[51] P. Datta, A. Barui, Y. Wu, V. Ozbolat, K.K. Moncal, IT. Ozbolat, Essential steps in bioprinting: from pre- to post-bioprinting, Biotechnol. Adv. 36 (2018) 1481–1504, https://doi.org/10.1016/J.BIOTECHADV.2018.06.003.
[52] A.N. Leberfinger, D.J. Ravnic, A. Dhawan, I.T. Ozbolat, Concise review: bioprinting of stem cells for transplantable tissue fabrication, Stem Cells Transl. Med. 6 (2017) 1940–1948, https://doi.org/10.1002/SCTM.17-0148.
[53] I.T. Ozbolat, M. Hospodiuk, Current advances and future perspectives in extrusion-based bioprinting, Biomaterials 76 (2016) 321–343, https://doi.org/10.1016/J.BIOMATERIALS.2015.10.076.
[54] J. Zhang, Q. Hu, S. Wang, J. Tao, M. Gou, Digital light processing based three-dimensional printing for medical applications, Int. J. Bioprint. 6 (2019) 12–27, https://doi.org/10.18063/IJB.V6I1.242.
[55] A. Van de Walle, J.E. Perez, C. Wilhelm, Magnetic bioprinting of stem cell-based tissues, Bioprinting 30 (2023) e00265, https://doi.org/10.1016/J.BPRINT.2023.E00265.
[56] R. Raman, R. Bashir, Stereolithographic 3D Bioprinting for Biomedical Applications. Essentials of 3D Biofabrication and Translation, Academic Press, 2015, pp. 89–121, https://doi.org/10.1016/B978-0-12-800972-7.00006-2.
[57] H. Gudapati, M. Dey, I. Ozbolat, A comprehensive review on droplet-based bioprinting: past, present and future, Biomaterials 102 (2016) 20–42, https://doi.org/10.1016/J.BIOMATERIALS.2016.06.012.
[58] J. Liu, M. Shahriar, H. Xu, C. Xu, Cell-laden bioink circulation-assisted inkjet-based bioprinting to mitigate cell sedimentation and aggregation, Biofabrication 14 (2022), https://doi.org/10.1088/1758-5090/AC8FB7, 045020.
[59] X. Li, B. Liu, B. Pei, J. Chen, D. Zhou, J. Peng, et al., Inkjet bioprinting of biomaterials, Chem. Rev. 120 (2020) 10793–10833, https://doi.org/10.1021/ACS.CHEMREV.0C00008.
[60] A. Zennifer, A. Subramanian, S. Sethuraman, Design considerations of bioinks for laser bioprinting technique towards tissue regenerative applications, Bioprinting 27 (2022) e00205, https://doi.org/10.1016/J.BPRINT.2022.E00205.
[61] M.A. Heinrich, W. Liu, A. Jimenez, J. Yang, A. Akpek, X. Liu, et al., 3D bioprinting: from benches to translational applications, Small 15 (2019), 1805510, https://doi.org/10.1002/SMLL.201805510.
[62] T.M. Valentin, S.E. Leggett, P.Y. Chen, J.K. Sodhi, L.H. Stephens, H. D. McClintock, et al., Stereolithographic printing of ionically-crosslinked alginate hydrogels for degradable biomaterials and microfluidics, Lab Chip 17 (2017) 3474–3488, https://doi.org/10.1039/C7LC00694B.
[63] F. Pati, J. Jang, J.W. Lee, D.W. Cho, Extrusion Bioprinting. Essentials of 3D Biofabrication and Translation, Academic Press, 2015, pp. 123–152, https://doi.org/10.1016/B978-0-12-800972-7.00007-4.
[64] R. Jamee, Y. Araf, N.I. bin, S.K. Promon, The promising rise of bioprinting in revolutionalizing medical science: advances and possibilities, Regen. Ther. 18 (2021) 133–145, https://doi.org/10.1016/J.RETH.2021.05.006.
[65] S. Derakhshanfar, R. Mbeleck, K. Xu, X. Zhang, W. Zhong, M. Xing, 3D bioprinting for biomedical devices and tissue engineering: a review of recent trends and advances, Bioact. Mater. 3 (2018) 144–156, https://doi.org/10.1016/J.BIOACTMAT.2017.11.008.
[66] E. Reina-Romo, S. Mandal, P. Amorim, V. Bloemen, E. Ferraris, L. Geris, Towards the experimentally-informed in silico nozzle design optimization for extrusion-based bioprinting of shear-thinning hydrogels, Front. Bioeng. Biotechnol. 9 (2021) 694, https://doi.org/10.3389/FBIOE.2021.701778.
[67] Y. Zhao, Y. Li, S. Mao, W. Sun, R. Yao, The influence of printing parameters on cell survival rate and printability in microextrusion-based 3D cell printing technology, Biofabrication 7 (2015), https://doi.org/10.1088/1758-5090/7/4/045002.
[68] P.S. Ginestra, R. Rovetta, A. Fiorentino, E. Ceretti, Bioprinting process optimization: evaluation of parameters influence on the extrusion of inorganic polymers, Procedia CIRP 89 (2020) 104–109, https://doi.org/10.1016/J.PROCIR.2020.05.125.
[69] E. Mancha Sánchez, J.C. Gómez-Blanco, E. López Nieto, J.G. Casado, A. Macías-García, M.A. Díaz Díez, et al., Hydrogels for bioprinting: a systematic review of hydrogels synthesis, bioprinting parameters, and bioprinted structures behavior, Front. Bioeng. Biotechnol. 8 (2020) 776, https://doi.org/10.3389/FBIOE.2020.00776.
[70] Fisch P., Holub M., Zenobi-Wong M. Improved accuracy and precision of bioprinting through progressive cavity pump-controlled extrusion. BioRxiv 2020: 2020.01.23.915868. doi:10.1101/2020.01.23.915868.
[71] I.P. Magalhães, P.M. de Oliveira, J. Dernowsek, C.E.B. las, C.M.S. Las, Investigation of the effect of nozzle design on rheological bioprinting properties using computational fluid dynamics, Matéria 24 (2019), https://doi.org/10.1590/S1517-707620190003.0714 (Rio de Janeiro).
[72] Ž.P. Kačarević, P.M. Rider, S. Alkildani, S. Retnasingh, R. Smeets, O. Jung, et al., An introduction to 3D bioprinting: possibilities, challenges and future aspects, Materials 11 (2018) 2199, https://doi.org/10.3390/MA11112199. Page 2199-201811.
[73] W.L. Ng, J.M. Lee, W.Y. Yeong, M. Win Naing, Microvalve-based bioprinting – process, bio-inks and applications, Biomater. Sci. 5 (2017) 632–647, https://doi.org/10.1039/C6BM00861E.
[74] K. Nair, M. Gandhi, S. Khalil, K.C. Yan, M. Marcolongo, K. Barbee, et al., Characterization of cell viability during bioprinting processes, Biotechnol. J. 4 (2009) 1168–1177, https://doi.org/10.1002/BIOT.200900004.
[75] J. Lewicki, J. Bergman, C. Kerins, O. Hermanson, Optimization of 3D bioprinting of human neuroblastoma cells using sodium alginate hydrogel, Bioprinting 16 (2019) e00053, https://doi.org/10.1016/J.BPRINT.2019.E00053.
[76] N. Thattaruparambil Raveendran, C. Vaquette, C. Meinert, D. Samuel Ipe, S. Ivanovski, Optimization of 3D bioprinting of periodontal ligament cells, Dent. Mater. 35 (2019) 1683–1694, https://doi.org/10.1016/J.DENTAL.2019.08.114.
[77] E. Núñez, E.W. Steyerberg, J. Núñez, Regression modeling strategies, Rev. Esp. Cardiol. (Engl. Ed.) 64 (2011) 501–507, https://doi.org/10.1016/J.REC.2011.01.017.
[78] S. Friedenthal, A. Moore, R. Steiner, Integrating SysML into a Systems Development Environment. A Practical Guide to SysML, Morgan Kaufmann, 2012, pp. 523–556, https://doi.org/10.1016/B978-0-12-385206-9.00018-1.
[79] S.S. Sidharth, Curve Fitting Simplified: Exploring the Intuitive Features of CurvPy (2023), doi:10.48550/arXiv.2307.06377.
[80] M. Wazid, A.K. Das, V. Chamola, Y. Park, Uniting cyber security and machine learning: advantages, challenges and future research, ICT Express 8 (2022) 313–321, https://doi.org/10.1016/J.ICTE.2022.04.007.
[81] A. Malekpour, X. Chen, Printability and cell viability in extrusion-based bioprinting from experimental, computational, and machine learning views, J. Funct. Biomater. 13 (2022) 40, https://doi.org/10.3390/JFB13020040. Page 40 2022;13.
[82] J. Karvinen, M. Kellomäki, Design aspects and characterization of hydrogel-based bioinks for extrusion-based bioprinting, Bioprinting 32 (2023) e00274, https://doi.org/10.1016/J.BPRINT.2023.E00274.
[83] S. Arjoca, A. Robu, M. Neagu, A. Neagu, Mathematical and computational models in spheroid-based biofabrication, Acta Biomater. 165 (2023) 125–139, https://doi.org/10.1016/J.ACTBIO.2022.07.024.
[84] D.V. Krishna, M.R. Sankar, Extrusion based bioprinting of alginate based multicomponent hydrogels for tissue regeneration applications: state of the art, Mater. Today Commun. 35 (2023), 105696, https://doi.org/10.1016/J.MTCOMM.2023.105696.
[85] X. Huang, W.L. Ng, W.Y. Yeong, Predicting the number of printed cells during inkjet-based bioprinting process based on droplet velocity profile using machine learning approaches, J. Intell. Manuf. (2023) 1–16, https://doi.org/10.1007/S10845-023-02167-4/FIGURES/10.
[86] J. Sun, K. Yao, K. Huang, D. Huang, Machine learning applications in scaffold based bioprinting, Mater. Today Proc. 70 (2022) 17–23, https://doi.org/10.1016/J.MATPR.2022.08.485.
[87] J. Sun, K. Yao, J. An, L. Jing, K. Huang, D. Huang, Machine learning and 3D bioprinting, Int. J. Bioprint. 9 (2023) 1–14, https://doi.org/10.18063/IJB.717.
[88] J. Shin, Y. Lee, Z. Li, J. Hu, S.S. Park, K. Kim, Optimized 3D bioprinting technology based on machine learning: a review of recent trends and advances, Micromachines 13 (2022) 363, https://doi.org/10.3390/MI13030363. Page 363 202213.
[89] K. Tröndle, G. Miotto, L. Rizzo, R. Pichler, F. Koch, P. Koltay, et al., Deep learning-assisted nephrotoxicity testing with bioprinted renal spheroids, Int. J. Bioprint. 8 (2022) 164–173, https://doi.org/10.18063/IJB.V8I2.528.
[90] T.G. Ritto, F.A. Rochinha, Digital twin, physics-based model, and machine learning applied to damage detection in structures, Mech. Syst. Signal Process. 155 (2021), 107614, https://doi.org/10.1016/J.YMSSP.2021.107614.
[91] L. Wang, M.E. Xu, L. Luo, Y. Zhou, P. Si, Iterative feedback bio-printing-derived cell-laden hydrogel scaffolds with optimal geometrical fidelity and cellular controllability, Sci. Rep. 8 (1) (2018) 1–13, https://doi.org/10.1038/s41598-018-21274-4, 2018 8.
[92] M. Guvendiren, H.D. Lu, J.A. Burdick, Shear-thinning hydrogels for biomedical applications, Soft Matter 8 (2011) 260–272, https://doi.org/10.1039/C1SM06513K.
[93] J.M. Townsend, E.C. Beck, S.H. Gehrke, C.J. Berkland, M.S. Detamore, Flow behavior prior to crosslinking: the need for precursor rheology for placement of hydrogels in medical applications and for 3D bioprinting, Prog. Polym. Sci. 91 (2019) 126–140, https://doi.org/10.1016/J.PROGPOLYMSCI.2019.01.003.
[94] M.M. de Santis, H.N. Alsafadi, S. Tas, D.A. Bölükbas, S. Prithiviraj, I.A.N. da Silva, et al., Extracellular-matrix-reinforced bioinks for 3D bioprinting human tissue, Adv. Mater. 33 (2021), 2005476, https://doi.org/10.1002/ADMA.202005476.
[95] N. Marx, L. Fernández, F. Barceló, H. Spikes, Shear thinning and hydrodynamic friction of viscosity modifier-containing oils. part I: shear thinning behaviour, Tribol. Lett. 66 (2018) 1–14, https://doi.org/10.1007/S11249-018-1039-5.
[96] M.M. Simpson, W.S. Janna, Newtonian and Non-Newtonian fluids: velocity profiles, viscosity data, and laminar flow friction factor equations for flow in a circular duct, in: Proceedings of the ASME International Mechanical Engineering Congress and Exposition 9, 2009, pp. 173–180, https://doi.org/10.1115/IMECE2008-67611.
[97] D. Chimene, C.W. Peak, J.L. Gentry, J.K. Carrow, L.M. Cross, E. Mondragon, et al., Nanoengineered ionic-covalent entanglement (NICE) bioinks for 3D bioprinting, ACS Appl. Mater. Interfaces 10 (2018) 9957–9968, https://doi.org/10.1021/ACSAMI.7B19808.
[98] J. Emmermacher, D. Spura, J. Cziommer, D. Kilian, T. Wollborn, U. Fritsching, et al., Engineering considerations on extrusion-based bioprinting: interactions of material behavior, mechanical forces and cells in the printing needle, Biofabrication 12 (2020), https://doi.org/10.1088/1758-5090/AB7553.
[99] M.E. Prendergast, M.D. Davidson, J.A. Burdick, A biofabrication method to align cells within bioprinted photocrosslinkable and cell-degradable hydrogel

constructs via embedded fibers, Biofabrication 13 (2021), https://doi.org/10.1088/1758-5090/AC25CC.
[100] J. Adhikari, M.S. Perwez, A. Das, P. Saha, Development of hydroxyapatite reinforced alginate–chitosan based printable biomaterial-ink, Nano-Struct. Nano-Objects 25 (2021), https://doi.org/10.1016/J.NANOSO.2020.100630.
[101] M.M. Lübtow, M. Mrlik, L. Hahn, A. Altmann, M. Beudert, T. Lühmann, et al., Temperature-dependent rheological and viscoelastic investigation of a poly(2-methyl-2-oxazoline)-b-poly(2-iso-butyl-2-oxazoline)-b-poly(2-methyl-2-oxazoline)-based thermogelling hydrogel, J. Funct. Biomater. 10 (2019) 36, https://doi.org/10.3390/JFB10030036. Page 36 201910.
[102] H. Zhang, Y. Cong, A. Rosemary Osi, Y. Zhou, F. Huang, R.P. Zaccaria, et al., Direct 3D printed biomimetic scaffolds based on hydrogel microparticles for cell spheroid growth, Adv. Funct. Mater. 30 (2020), 1910573, https://doi.org/10.1002/ADFM.201910573.
[103] H. Huang, D. Dean, 3-D printed porous cellulose acetate tissue scaffolds for additive manufacturing, Addit. Manuf. 31 (2020), 100927, https://doi.org/10.1016/J.ADDMA.2019.100927.
[104] A. Pössl, D. Hartzke, T.M. Schmidts, F.E. Runkel, P. Schlupp, A targeted rheological bioink development guideline and its systematic correlation with printing behavior, Biofabrication 13 (2021), https://doi.org/10.1088/1758-5090/ABDE1E.
[105] S.J. Müller, E. Mirzahossein, E.N. Iftekhar, C. Bächer, S. Schrüfer, D.W. Schubert, et al., Flow and hydrodynamic shear stress inside a printing needle during biofabrication, PLoS ONE 15 (2020), https://doi.org/10.1371/JOURNAL.PONE.0236371.
[106] S. Xin, K.A. Deo, J. Dai, N.K.R. Pandian, D. Chimene, R.M. Moebius, et al., Generalizing hydrogel microparticles into a new class of bioinks for extrusion bioprinting, Sci. Adv. 7 (2021) 3087–3102, https://doi.org/10.1126/SCIADV.ABK3087.
[107] S. Zhang, G. Li, J. Man, S. Zhang, J. Li, J. Li, et al., Fabrication of microspheres from high-viscosity bioink using a novel microfluidic-based 3D bioprinting nozzle, Micromachines 11 (2020) 681, https://doi.org/10.3390/MI11070681. Vol 11, Page 681 2020.
[108] M. Bartnikowski, R.M. Wellard, M. Woodruff, T. Klein, Tailoring hydrogel viscoelasticity with physical and chemical crosslinking, Polymers 7 (2015) 2650–2669, https://doi.org/10.3390/POLYM7121539, 2015;7:2650–69.
[109] S. Das, F. Pati, Y.J. Choi, G. Rijal, J.H. Shim, S.W. Kim, et al., Bioprintable, cell-laden silk fibroin-gelatin hydrogel supporting multilineage differentiation of stem cells for fabrication of three-dimensional tissue constructs, Acta Biomater. 11 (2015) 233–246, https://doi.org/10.1016/J.ACTBIO.2014.09.023.
[110] J.C. Gómez-Blanco, E. Mancha-Sánchez, A.C. Marcos, M. Matamoros, A. Díaz-Parralejo, J.B. Pagador, Bioink temperature influence on shear stress, pressure and velocity using computational simulation, in: Processes, 8, 2020, p. 865, https://doi.org/10.3390/PR8070865. Page 865 2020;8.
[111] T. Jain, H.B. Baker, A. Gipsov, J.P. Fisher, A. Joy, D.S. Kaplan, et al., Impact of cell density on the bioprinting of gelatin methacrylate (GelMA) bioinks, Bioprinting 22 (2021) e00131, https://doi.org/10.1016/J.BPRINT.2021.E00131.
[112] Q. Li, B. Zhang, Q. Xue, C. Zhao, Y. Luo, H. Zhou, et al., A systematic thermal analysis for accurately predicting the extrusion printability of alginate-gelatin-based hydrogel bioinks, Int. J. Bioprint. 7 (2021) 108–123, https://doi.org/10.18063/IJB.V7I3.394.
[113] Y. Sümbelli, S.E. Diltemiz, M.G. Say, Ö.B. Ünlüer, A. Ersöz, R. Say, *In situ* and non-cytotoxic cross-linking strategy for 3D printable biomaterials, Soft Matter 17 (2021) 1008–1015, https://doi.org/10.1039/D0SM01734E.
[114] A. Gebeyehu, S.K. Surapaneni, J. Huang, A. Mondal, V.Z. Wang, N.F. Haruna, et al., Polysaccharide hydrogel based 3D printed tumor models for chemotherapeutic drug screening, Sci. Rep. 11 (2021) 1–15, https://doi.org/10.1038/s41598-020-79325-8, 2021 11:1.
[115] A. Lúcia Gabas, R. Alexandre, F. Cabral, C.A. Fernandes De Oliveira, J. Telis-Romero, Density and rheological parameters of goat milk, Food Sci. Technol. 32 (2012) 381–385, https://doi.org/10.1590/S0101-20612012005000033.
[116] B. Abu-Jdayil, R.Y. Jumah, RR. Shaker, Rheological properties of a concentrated fermented product, labneh, produced from bovine milk: effect of production method, Int. J. Food Prop. 5 (2002) 667–679, https://doi.org/10.1081/JFP-120015500.
[117] M.E. Cooke, D.H. Rosenzweig, The rheology of direct and suspended extrusion bioprinting, APL Bioeng. 5 (2021), https://doi.org/10.1063/5.0031475.
[118] L. Ouyang, R. Yao, Y. Zhao, W. Sun, Effect of bioink properties on printability and cell viability for 3D bioplotting of embryonic stem cells, Biofabrication 8 (2016), https://doi.org/10.1088/1758-5090/8/3/035020.
[119] S. Knowlton, B. Yenilmez, S. Anand, S. Tasoglu, Photocrosslinking-based bioprinting: examining crosslinking schemes, Bioprinting 5 (2017) 10–18, https://doi.org/10.1016/J.BPRINT.2017.03.001.
[120] M.G. Haugh, C.M. Murphy, R.C. McKiernan, C. Altenbuchner, F.J. O'Brien, Crosslinking and mechanical properties significantly influence cell attachment, proliferation, and migration within collagen glycosaminoglycan scaffolds, Tissue Eng. Part A 17 (2011) 1201–1208, https://doi.org/10.1089/TEN.TEA.2010.0590.
[121] C.C. Piras, D.K. Smith, Multicomponent polysaccharide alginate-based bioinks, J. Mater. Chem. B 8 (2020) 8171–8188, https://doi.org/10.1039/D0TB01005G.
[122] I. Fernández Farrés, I.T. Norton, Formation kinetics and rheology of alginate fluid gels produced by *in-situ* calcium release, Food Hydrocoll. 40 (2014) 76–84, https://doi.org/10.1016/J.FOODHYD.2014.02.005.
[123] K. Song, B. Ren, Y. Zhai, W. Chai, Y. Huang, Effects of transglutaminase cross-linking process on printability of gelatin microgel-gelatin solution composite bioink, Biofabrication 14 (2021), 015014, https://doi.org/10.1088/1758-5090/AC3D75.
[124] Q.Q. Wang, D.J. Chen, Determination of gelation kinetic parameters for a chitosan/β-glycerophosphate injectable hydrogel by means of rheological measurement, Mater. Sci. Forum 848 (2016) 543–550, https://doi.org/10.4028/WWW.SCIENTIFIC.NET/MSF.848.543.
[125] J. Xu, Y. Liu, H.S. Hui, Hydrogels based on schiff base linkages for biomedical applications, Molecules 24 (2019) 3005, https://doi.org/10.3390/MOLECULES24163005. Page 3005 201924.
[126] P. Vinchhi, S.U. Rawal, M.M Patel, Biodegradable hydrogels. Drug Delivery Devices and Therapeutic Systems, Academic Press, 2021, pp. 395–419, https://doi.org/10.1016/B978-0-12-819838-4.00012-2.
[127] W. Hu, Z. Wang, Y. Xiao, S. Zhang, J. Wang, Advances in crosslinking strategies of biomedical hydrogels, Biomater. Sci. 7 (2019) 843–855, https://doi.org/10.1039/C8BM01246F.
[128] H. Hecht, S. Srebnik, Structural characterization of sodium alginate and calcium alginate, Biomacromolecules 17 (2016) 2160–2167, https://doi.org/10.1021/ACS.BIOMAC.6B00378.
[129] L. Mengatto, M.G. Ferreyra, A. Rubiolo, I. Rintoul, J. Luna, Hydrophilic and hydrophobic interactions in cross-linked chitosan membranes, Mater. Chem. Phys. 139 (2013) 181–186, https://doi.org/10.1016/J.MATCHEMPHYS.2013.01.019.
[130] G.M. ter Huurne, I.K. Voets, A.R.A. Palmans, E.W. Meijer, Effect of intra- versus intermolecular cross-linking on the supramolecular folding of a polymer chain, Macromolecules 51 (2018) 8853–8861, https://doi.org/10.1021/ACS.MACROMOL.8B01623.
[131] K. Hölzl, S. Lin, L. Tytgat, S. van Vlierberghe, L. Gu, A. Ovsianikov, Bioink properties before, during and after 3D bioprinting, Biofabrication 8 (2016), https://doi.org/10.1088/1758-5090/8/3/032002.
[132] N. Ashammakhi, S. Ahadian, C. Xu, H. Montazerian, H. Ko, R. Nasiri, et al., Bioinks and bioprinting technologies to make heterogeneous and biomimetic tissue constructs, Mater. Today Bio 1 (2019), 100008, https://doi.org/10.1016/J.MTBIO.2019.100008.
[133] A. Ghavaminejad, N. Ashammakhi, X.Y. Wu, A. Khademhosseini, A. Ghavaminejad, X.Y. Wu, et al., Crosslinking strategies for 3D bioprinting of polymeric hydrogels, Small 16 (2020), 2002931, https://doi.org/10.1002/SMLL.202002931.
[134] S. Boularaoui, G. Hussein, K.A. Khan, N. Christoforou, C. Stefanini, An overview of extrusion-based bioprinting with a focus on induced shear stress and its effect on cell viability, Bioprinting 20 (2020), https://doi.org/10.1016/J.BPRINT.2020.E00093.
[135] K. Thakare, L. Jerpseth, H. Qin, Z. Pei, Bioprinting using algae: effects of extrusion pressure and needle diameter on cell quantity in printed samples, J. Manuf. Sci. Eng. Trans. ASME 143 (2021), https://doi.org/10.1115/1.4048853/1088920.
[136] M. Aliabouzar, A.W.Y. Ley, S. Meurs, A.J. Putnam, B.M. Baker, O.D. Kripfgans, et al., Micropatterning of acoustic droplet vaporization in acoustically-responsive scaffolds using extrusion-based bioprinting, Bioprinting 25 (2022) e00188, https://doi.org/10.1016/J.BPRINT.2021.E00188.
[137] K.H. Kang, L.A. Hockaday, J.T. Butcher, Quantitative optimization of solid freeform deposition of aqueous hydrogels, Biofabrication 5 (2013), https://doi.org/10.1088/1758-5082/5/3/035001.
[138] Z. Gu, J. Fu, H. Lin, Y. He, Development of 3D bioprinting: from printing methods to biomedical applications, Asian J. Pharm. Sci. 15 (2020) 529–557, https://doi.org/10.1016/J.AJPS.2019.11.003.
[139] R. Attalla, C. Ling, P. Selvaganapathy, Fabrication and characterization of gels with integrated channels using 3D printing with microfluidic nozzle for tissue engineering applications, Biomed. Microdevices 18 (2016) 1–12, https://doi.org/10.1007/S10544-016-0042-6.
[140] Y. Wang, W.D. Müller, A. Rumjahn, A. Schwitalla, Parameters influencing the outcome of additive manufacturing of tiny medical devices based on PEEK, Materials 13 (2020) 466, https://doi.org/10.3390/MA13020466. Vol 13, Page 466 2020.
[141] A. Kjar, B. McFarland, K. Mecham, N. Harward, Y. Huang, Engineering of tissue constructs using coaxial bioprinting, Bioact. Mater. 6 (2021) 460–471, https://doi.org/10.1016/J.BIOACTMAT.2020.08.020.
[142] E.A. Heile, E.R. Komosa, B.M. Ogle, A simple methodology for determining optimal print parameters for 3D bioprinting with low-viscosity bioink, Minn. Undergrad. Res. Acad. J. 4 (2021) 1–12.
[143] K. Fakhruddin, M.S.A. Hamzah, S.I.A. Razak, Effects of extrusion pressure and printing speed of 3D bioprinted construct on the fibroblast cells viability, IOP Conf. Ser. Mater. Sci. Eng. (Online) 440 (2018), https://doi.org/10.1088/1757-899X/440/1/012042.
[144] M. Hospodiuk, K.K. Moncal, M. Dey, I.T. Ozbolat, Extrusion-Based Biofabrication in Tissue Engineering and Regenerative Medicine. 3D Printing and Biofabrication, Springer Cham, 2018, pp. 255–281, https://doi.org/10.1007/978-3-319-45444-3_10.
[145] Z. Jin, Z. Zhang, X. Shao, G.X. Gu, Monitoring anomalies in 3D bioprinting with deep neural networks, ACS Biomater. Sci. Eng. (2021), https://doi.org/10.1021/ACSBIOMATERIALS.0C01761.
[146] K.H. Kang, L.A. Hockaday, J.T. Butcher, Quantitative optimization of solid freeform deposition of aqueous hydrogels, Biofabrication 5 (2013), 035001, https://doi.org/10.1088/1758-5082/5/3/035001.
[147] I.T. Ozbolat, Extrusion-Based Bioprinting ** with minor contributions by Monika Hospodiuk, The Pennsylvania State University, 3D Bioprinting (2017) 93–124, https://doi.org/10.1016/B978-0-12-803010-3.00004-4.
[148] L. Ning, N. Betancourt, D.J. Schreyer, X. Chen, Characterization of cell damage and proliferative ability during and after bioprinting, ACS Biomater. Sci. Eng. 4 (2018) 3906–3918, https://doi.org/10.1021/ACSBIOMATERIALS.8B00714.

[149] S.Y. Nam, S.H. Park, ECM based bioink for tissue mimetic 3D bioprinting, Adv. Exp. Med. Biol. 1064 (2018) 335–353, https://doi.org/10.1007/978-981-13-0445-3_20.
[150] R. Suntornnond, E.Y.S. Tan, J. An, C.K. Chua, A mathematical model on the resolution of extrusion bioprinting for the development of new bioinks, Materials 9 (2016), https://doi.org/10.3390/MA9090756 (Basel).
[151] D. Trucco, A. Sharma, C. Manferdini, E. Gabusi, M. Petretta, G. Desando, et al., Modeling and fabrication of silk fibroin-gelatin-based constructs using extrusion-based three-dimensional bioprinting, ACS Biomater. Sci. Eng. 7 (2021) 3306–3320, https://doi.org/10.1021/ACSBIOMATERIALS.1C00410.
[152] S. Ji, M. Guvendiren, Complex 3D bioprinting methods, APL Bioeng. 5 (2021), https://doi.org/10.1063/5.0034901.
[153] M.L. Bedell, J.L. Guo, V.Y. Xie, A.M. Navara, A.G. Mikos, Polymer scaffold fabrication, Princ. Tissue Eng. (2020) 295–315, https://doi.org/10.1016/B978-0-12-818422-6.00018-6.
[154] L. Lucas, A. Aravind, P. Emma, M. Christophe, E.J.C. Rheology, simulation and data analysis toward bioprinting cell viability awareness, Bioprinting 21 (2021) e00119, https://doi.org/10.1016/J.BPRINT.2020.E00119.
[155] Rakić T., Kasagić-Vujanović I., Jovanović M., Jančić-Stojanović B., Ivanović D. Comparison of full factorial design, central composite design, and box-behnken design in chromatographic method development for the determination of fluconazole and its impurities. 2014;47:1334–47. doi:10.1080/00032719.2013.867503.
[156] Heckert N.A., Filliben J.J., Croarkin C.M., Hembree B., Guthrie W.F., Tobias P., et al. Handbook 151: NIST/SEMATECH e-Handbook of Statistical Methods. NIST Interagency/Internal Report (NISTIR) 2002.
[157] J. Shi, J. Song, B. Song, W.F. Lu, Multi-objective optimization design through machine learning for drop-on-demand bioprinting, Engineering 5 (2019) 586–593, https://doi.org/10.1016/J.ENG.2018.12.009.
[158] F.Y. Cheng, Multiobjective optimum design of structures with genetic algorithm and game theory: application to life-cycle cost design, Comput. Mech. Struct. Eng. (1999) 1–16, https://doi.org/10.1016/B978-008043008-9/50039-9.
[159] Dumas R., Moissenet F., Lafon Y., Cheze L. Multi-objective optimisation for musculoskeletal modelling: application to a planar elbow model. 2014;228:1108–13. doi:10.1177/0954411914556790.